Silicon (2024) 16:485–511
https://doi.org/10.1007/s12633-023-02723-w

REVIEW

Recent Advances and Prospects in Silicon Nanowire Sensors: A Critical Review

S. Sreejith[1] · J. Ajayan[2] · N. V. Uma Reddy[1] · M. Manikandan[3]

Received: 8 August 2023 / Accepted: 8 October 2023 / Published online: 21 October 2023
© The Author(s), under exclusive licence to Springer Nature B.V. 2023

Abstract
Due to the distinctive optical, mechanical and electrical characteristics, silicon nanowire (SilNW), one of the one dimensional nanostructures, has become a potential sensing nanomaterial. SilNWs have drawn interest in high-sensitive sensor fabrication, primarily because of their large surface-volume ratios, which significantly enhanced the detection limit to femtomolar concentrations and also provided high sensitivity. Due to its high charge sensitivity, SilNW FET-based sensors had been employed extensively for sensing various chemical as well as biological species. In this work, the sensing performance and applications of different SilNW biosensors, gas sensors, chemical and metal ion sensors were studied. In this study, we have also elaborated the most current developments as well as the sensing performance of various SilNW-based Covid-19 sensors.

Keywords Silicon nanowire sensors · Silicon nanowire bio-sensors · Gas sensors · Chemical sensors · pH sensors · Silicon nanowire humidity sensors · Metal-ion sensors · Covid-19 sensors

1 Introduction

Nanowires are structures which facilitate both flexibility as well as miniaturization, have exhibited substantial potential as sensor component in various electronic sensing devices. SilNW being key nanostructure has been a subject of research since 1950s, have emerged as an ideal candidate to be used as sensing element due to its 1-dimensional quasi electronic structure and their large surface-volume ratio. SilNWs also find application in photovoltaics, lithium-ion battery anodes, field-effect transistors, thermoelectrics etc. [1–5]. By varying the doping process condition, the conductance of SilNW can be adjusted so as to enhance its sensitivity. As a way to enhance surface area which is exposed to target molecules, SilNW can be made suspended, which will further improve its sensitivity. Another advantage of using SilNW is its compatibility with classical Sil technology as easy integration of peripheral circuitry on the same chip can be achieved [6–15]. SilNWs are usually fabricated using two approaches namely bottom up and top down. In top down fabrication approach SilNW is fabricated using lithographic process by scaling down bulk Sil wafer to the desired size and shape. Fig. 1 represents the schematic of a top-down SilNW device fabrication process. The fabrication of SilNW devices is carried out on the SOI (Sil on insulator) platform having oxide buried layer. In order to pattern the nanowire structure on the silicon-on-insulator layer, electron beam lithography was used. By applying anisotropic and isotropic etching, SilNWs can be made suspended. Bottom up method (metal assisted chemical etching, oxide assisted growth, vapour liquid solid) is a SilNW synthesize or growth technique from bulk Sil wafer via catalyzed metal-free or catalyzed metal -assisted process. Metal assisted chemical etching has been reported as an easy and low-cost process for SilNWs array manufacturing. This process consists of two major steps namely deposition of electroless metal on Sil wafer as well as chemical etching using solution based on fluoride-ion. In oxide assisted SilNW growth, SiO was used as a starting material to enhance the growth and nucleation of SilNWs without catalyzed metal assistance and resulted in high purity SilNWs devoid of metal contamination.

✉ S. Sreejith
sreejith5488@gmail.com

[1] Department of Artificial Intelligence and Machine Learning, New Horizon College of Engineering, Bangalore, Karnataka, India

[2] Department of Electronics and Communication Engineering, SR University, Warangal, Telangana, India

[3] Department of Electronics and Communication Engineering, Presidency University, Bangalore, Karnataka, India

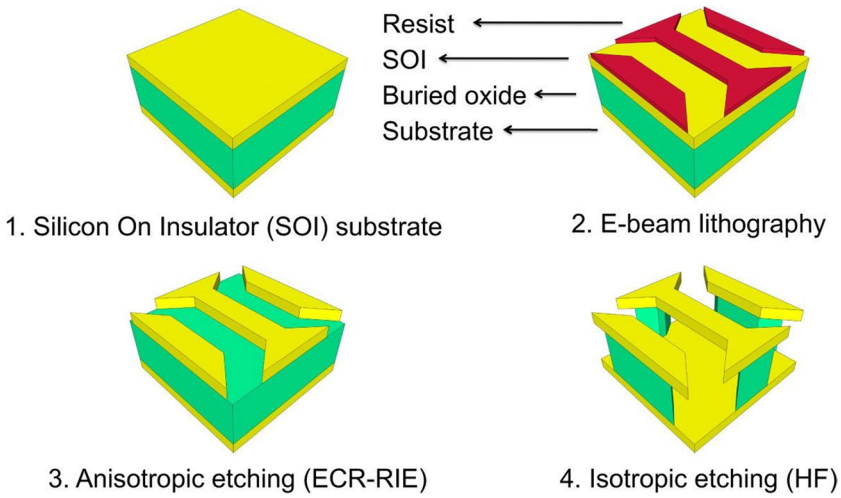

Fig. 1 Top-Down SilNW device fabrication process [25] (Copyright @ Elsevier)

Metal-catalyzed (Al, Fe, Pt, Au etc.) would be placed on the Sil wafer first in vapour liquid solid method and laser ablation or chemical vapour deposition procedures are used to accelerate SilNW development. [16–25].

In this article, we had elaborated briefly the sensing performance of various SilNW based biosensors, gas sensors, chemical and metal ion sensors, pH sensors, humidity sensors, strain and pressure sensors and photonic sensors. The emerging application of SilNW sensors in rapid Covid-19 virus detection was also reviewed critically.

2 Silicon Nanowire Based Bio-Sensors

SilNW sensors are generally FET based sensors having gate, drain and source electrodes (Fig. 2). SilNW biosensor works by varying the current that flows through the SilNW channel, influenced by the variation in surface charges due to binding reaction of biomolecule. Due to its benefits like capability to integrate with complementary metal-oxide semiconductors, direct electrical readouts and good sensitivity, FET based SilNW sensors have exhibited a lot of potential in bio-sensing applications. [28–30].

In the year 2008, A.Cattani-Scholz et al. [31] investigated PNA functionalized organophosphonate-based SilNW sensor with self-assembled hydroxyalkylphosphonate monolayer interface system for label-free DNA sensing. Upon electrolyte 1μM DNA buffer solution injection, a decline in wire resistance value corresponding to variation in surface potential of approximately 1.5 mV was reported. In the year 2010, Guo-Jun Zhang et al. [32] reported SilNW sensor functionalized with reverse-transcription-polymerase chain reaction technique for label free, quick and high sensitive identification of dengue virus using electrical detection and nucleic acid hybridization (Fig. 3).

By computing the change of resistance in SilNW after and before the binding of the DEN-2 reverse-transcription-polymerase chain reaction product to the PNA sequence,

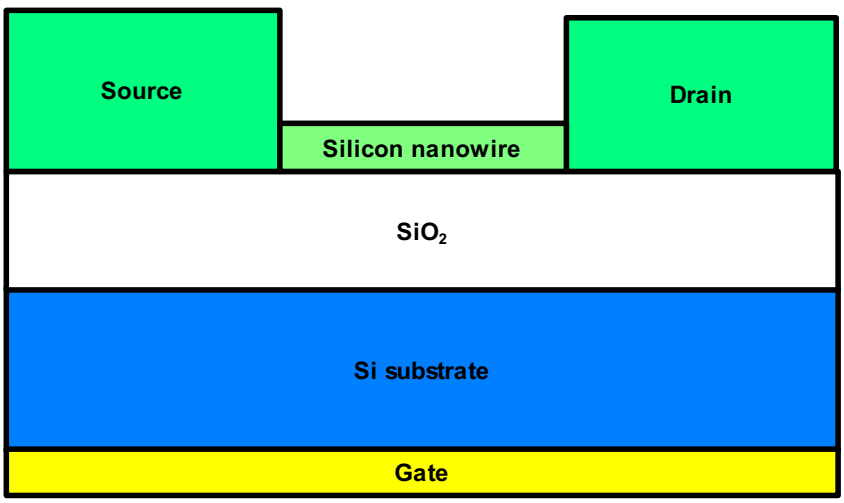

Fig. 2 Schematic representation of SilNW FET based biosensor [26, 27]

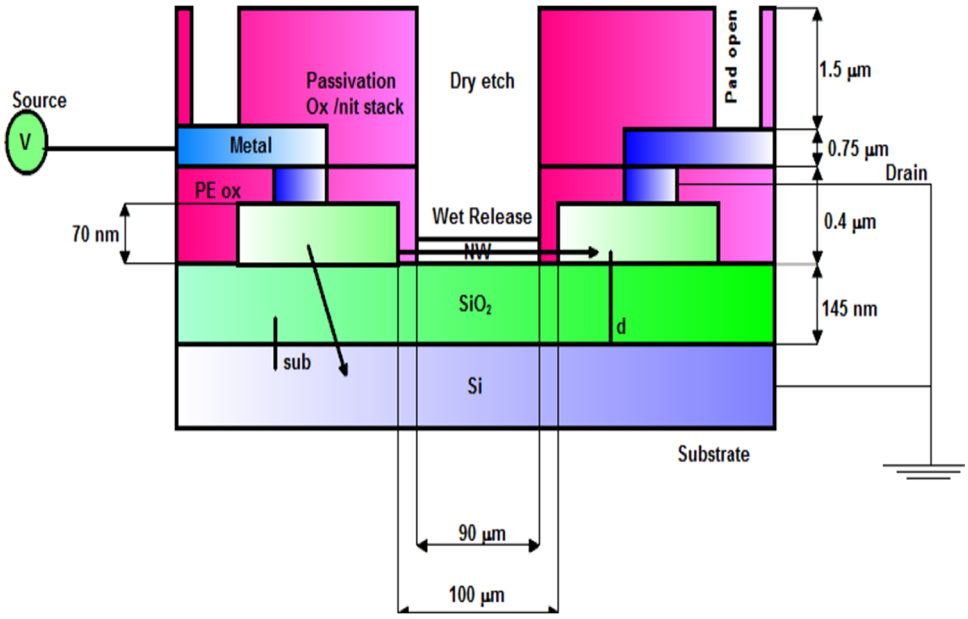

Fig. 3 Schematic illustration of SilNW FET based dengue virus detection biosensor [32]

detection limit below 10 fM for amplicons concentration in thirty minutes was reported. In the year 2010, Seong-Wan Ryu et al. [33] reported SilNW biosensor embedded with gold nanoparticle for high sensitive DNA label free sensing. In order to measure the probe oligonucleotides immobilization as well as its oligonucleotides target hybridization, the flow of electric current in between drain and source electrodes were measured. At a concentration of 1 pM, 23-mer oligonucleotide complementary target analogous to the DNA of breast cancer was reported in SilNW gold nanoparticle embedded biosensor. In the same year, Guo-Jun Zhang et al. [34] reported SilNW biosensor functionalized with Morpholino for label free and sequence specific DNA detection. Fluorescence microscopy and photoelectron X-ray spectroscopy were used for DNA-Morpholino hybridization and Morpholino attachment on to the surface of Sil. High specificity for DNA recognition was reported in Morpholino-modified surface and the SilNW sensor reported DNA detection in hundreds of femtomolar range. In 2011, D.H.Kwon et al. [35] reported SilNW modified by gold NPs using aminopropyltriethoxysilane self-assembled monolayer for sensing albumin. It was reported that the reliability of sensor got increased by repeated thermal treatment in vacuum, as it improves the conductivity from aminopropyltriethoxysilane molecule carbonization and also by making gold NPs in close contact to SilNW surface. SilNW modified with gold NPs array sensor reported range of detection of 1-7 µM for bovine serum albumin. In the same year, Guo-Jun Zhang et al. [36] reported monolayer-assisted self-assembled SilNW biosensor for DNA-protein interaction detection in breast cancer cells nuclear extracts. A self-assembled vinyl-terminated monolayer was applied to the SilNW surface, and oxidation transformed the surfaces termination into carboxylic acid. Atomic force microscopy and photoelectron X-ray spectroscopy were used to observe protein-DNA interaction on the SilNW surface and to characterize the step-by-step functionalization of the self-assembled monolayer and DNA on bare Sil surface. (ERE, dsDNA) estrogen receptor element and (ERα, protein) estrogen receptor alpha binding were used in the research. The sensor reported limit of detection as low as 10fM for detecting ERα. In the year 2012, A. Kulkarni et al. [37] reported SilNW array based sensor for selective and sensitive detection of as synthesized two dimensional DNA lattices with biotins. Top down approach was used to fabricate SilNW array which contains two fifty nanowires of twenty µm length spaced equally with an interval of 3.2 µm (Fig. 4).

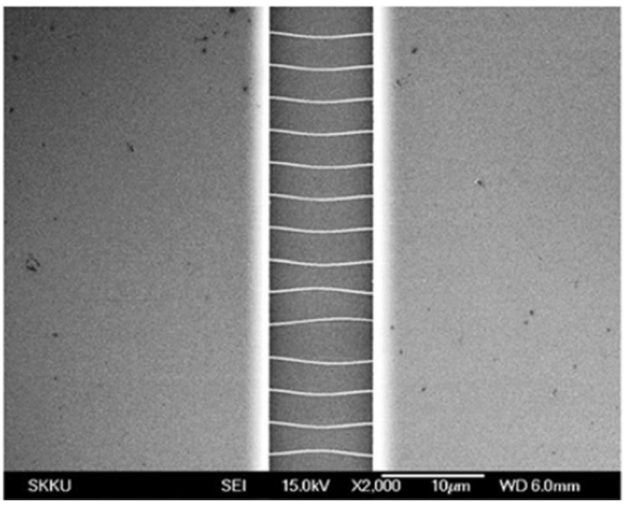

Fig. 4 Fabrication result of SilNW array [37] (Copyright @Elsevier)

It was reported that the SilNW responsivity peak, caused by optical local field enhancement linked to the dielectric periodic structure of the NWs exist at 480 nm in the photocurrent spectrum (Fig. 5). Further the photo-resistivity of the SilNW array device reported significant changes as a result of conductivity in DNA lattices with protein streptavidin, making it an ideal device for DNA detection and applications like toxic detection, DNA forensics and in immunological assays

In the year 2012, X. Duan et al. [38] investigated use of SilNW biosensors to study the ligand-protein binding affinities as well as kinetics and reported sensitivity down to fM concentrations. An analytical model was formed by combining device solution trans-conductance that can normalize the sensor response with Langmuir isotherms which can be used to measure binding-affinities of molecules (Eq. 1) [38].

$$\frac{\Delta I_{ds}}{g_m} = \Delta V_T = \frac{q_A}{C_0}\,[B]_{max}\ x\ \frac{[A]}{[A]+K_D} \tag{1}$$

where g_m represents trans-conductance, ΔV_T represents threshold voltage shift, q_A represents electric charge that is contributed by adsorbed analytes, K_D represents equilibrium constant, C_0 represents channel/analyte capacitive coupling, [A] represents bulk solution analyte concentration and $[B]_{max}$ represent the maximum functional binding sites surface density on the SilNW. In the year 2013, P. Serre et al. [39] reported DNA sensor in which random network based on SilNW was fabricated through low cost, versatile and simple vacuum filtration technique. The fabricated nanowire density can be monitored easily and also were homogeneous and reproducible. At room temperature these networks can be deposited on to various types of substrates. Through fluorescence it was demonstrated

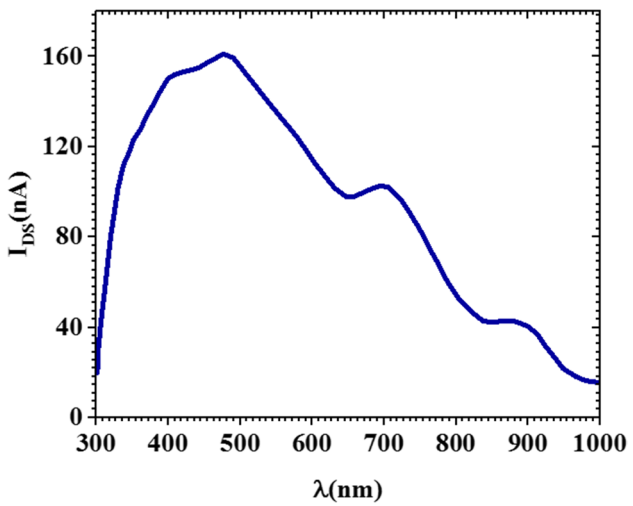

Fig. 5 Photocurrent spectral response of SilNW array chip [37]

that due to the nano-wire geometry, SilNW networks when compared to Si_3N_4 surface are extremely selective to DNA hybridization with an improved sensitivity and selectivity. In the same year Jia-Yo Wu et al. [40] reported SilNW back-gated FET based sensor for detecting a fragment of cancer-related (IL-1β) interleukin-1β gene. Plasma modification treatment was employed on device surface with various parameters to increase SilNW sensor sensitivity and it was reported that after one minute of N_2O plasma treatment, the sensitivity of SilNW FET sensor can be enhanced because after N_2O plasma treatment the detection region morphology was rougher. From the normalized current shift value, N_2O plasma-treated SilNW FET sensor reported sensitivity of 0.12/decade in sensing IL-1β 20-mer target DNA with 2.5 fM limit of detection. The normalized current shift was computed as [40]

$$I_{d,\text{normalized current shift}} = \left(I_{d,after} - I_{d,before}\right)/I_{d,before} \tag{2}$$

where $I_{d,after}$ represents drain current after injecting target DNA and $I_{d,before}$ represents drain current before injecting target DNA.

In the year 2014, H. Wang et al. [41] reported SilNW based fluorescent sensor for alkaline phosphatase detection. A number of phosphate compounds are hydrolyzed and transphosphorylated by alkaline phosphatase, which is a hydrolase phosphomonoester enzyme, to produce the appropriate alcohols and phosphate ions. Several diseases like prostatic and breast cancer, diabetes, liver dysfunction, bone disease etc. can be caused due to abnormal level of serum alkaline phosphatase. SilNW sensor was fabricated by immobilizing fluorescein molecules covalently on the surface of SilNWs along with phosphorylation of the fluorescein immobilized group. The SilNW fluorescent biosensor demonstrated a linear range of detection of 0.0175 U/mL–0.3U/mL with 0.0175 U/mL detection limit. The sensor also reported a response time of 20 minutes. The potential of SilNW fluorescent biosensor in measuring alkaline phosphatase was evident form the relative fluorescence intensity time curves (Fig. 6) in which by increasing the concentration of alkaline phosphatase, SilNW fluorescent biosensor exhibited higher level of fluorescence enhancement and faster enzymatic reaction rate. In the year 2014, G. Jayakumar et al. [42] reported pixel based fully electronic SilNW based biosensor with back gate and fluid gate on chip integrated with CMOS circuits. The side wall transfer lithography process were used to fabricate nanowires as it was time and cost efficient. The sensor consists of eight output-input pins and N by N pixel matrix. Single crystalline SilNW with cross-section area 75 by 20 nm was defined in each pixel. This design facilitates sequential readout of individual SilNWs and can be utilized for charge based instantaneous detection of molecules in gases or liquids. In the year 2015,

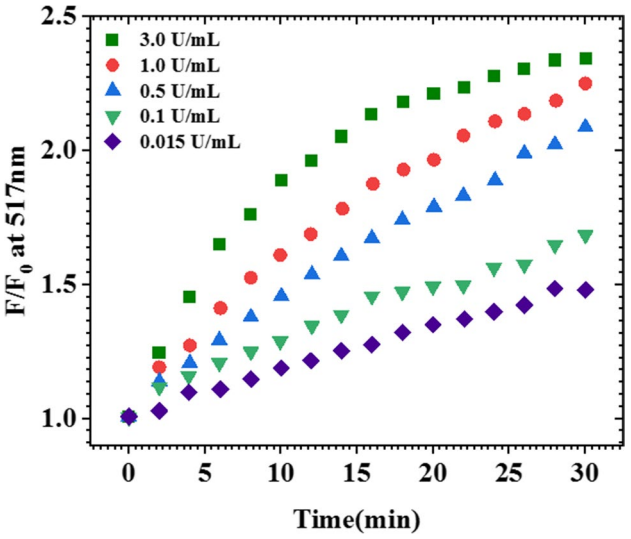

Fig. 6 Fluorescence-intensity time plot at 517 nm with different alkaline phosphatase concentrations [41]

Shih-Hsiang Shen et al. [43] reported multi-channel SilNW cardiac troponin I biosensor with stacked dielectric structure (Fig. 7) coated with high-k dielectric materials namely HfO_2 and Al_2O_3 for enhancing the sensing property. When compared to the performance of sensor with only high-k dielectric devices, SiO_2 ultrathin sensing membrane structure stacked with 10 nm HfO_2 and 14 nm Al_2O_3 reported enhanced sensing property of 1.4 and 3.8 times. The sensor reported 320 fM limit of detection along with 20% signal enhancement.

In the year 2015, T. Adam et al. [44] reported liquid gate control SilNW sensor for specific single-stranded DNA molecule detection which can be used in liquid environment. Conventional photolithography was used to fabricate the sensor and was coupled inductively with plasma dry etching process. In order to create a molecular binding chemistry, the sensor surface was salinized and subjected to (3-aminopropyl) triethoxysilane amination. The sensor reported high reusability and 0.1 nM limit of detection with a detection range of 100 pM to 25 nM. However it was observed that surface composition and nanowire size can limit the sensor response. The sensor response was be computed as [44]

$$\text{Device response} = \frac{G_{25} - G_{0.1}}{G_{25}} \times 100 \tag{3}$$

where G_{25} represents current response at 25 nM and $G_{0.1}$ represents current response at 0.1 nM. In the same year J. Lee et al. [45] reported SilNW based hybrid biosensor integrated with amplifier MOSFET fabricated via classical CMOS technology. It was observed that amplifier MOSFET integration will enhance FET based biosensors current response. The hybrid SilNW sensor for pH detection reported 5.74 decades per pH current response which when compared to single SilNW biosensor is 2.5×10^5 times larger. The sensor also exhibited 4.5×10^5 high current change for 500 nM concentration of poly(allylamine hydrochloride) charged polymer detection.

In the year 2016, Li-Chen Yen et al. [46] reported horn-like polycrystalline-SilNW FET biosensor for label free and real time sensing of ferritin protein. Spacer wire method was used to create a dummy gate trapezoidal-shaped structure that is used to fabricate nanowires which resemble horns. It was reported that horn-like poly-SilNW FET having 2 µm channel length exhibited good electrical characteristics (Fig. 8), increased I_{on}/I_{off} value of 3.47×10^5 and lesser threshold voltage value of 1.1 V in comparison with other channel lengths. Additionally, the sensor also exhibited 133.47 mV/pH high sensitivity value due to the large capacitive coupling ratio, exceeding Nernst limit. In the year 2016, S.F.A.Rahman et al. [47] reported oxygen plasma treated SilNW biosensor functionalized with standard complementary metal oxide- semiconductor process for detecting

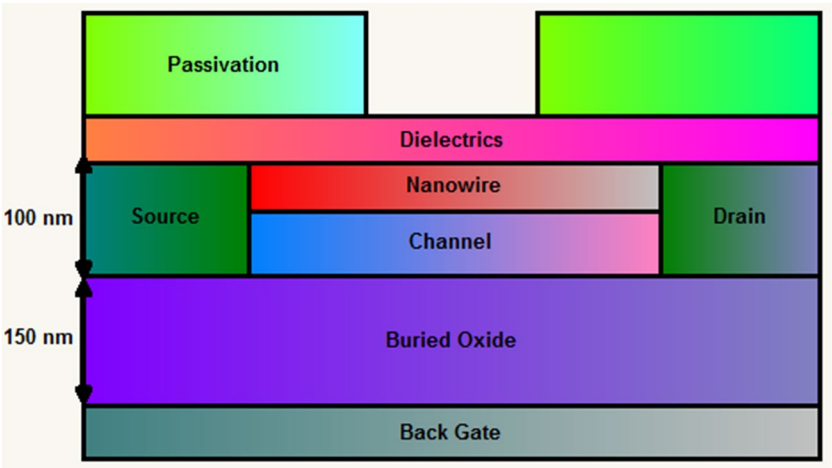

Fig. 7 Schematic illustration of SilNW cardiac troponin I biosensor [43]

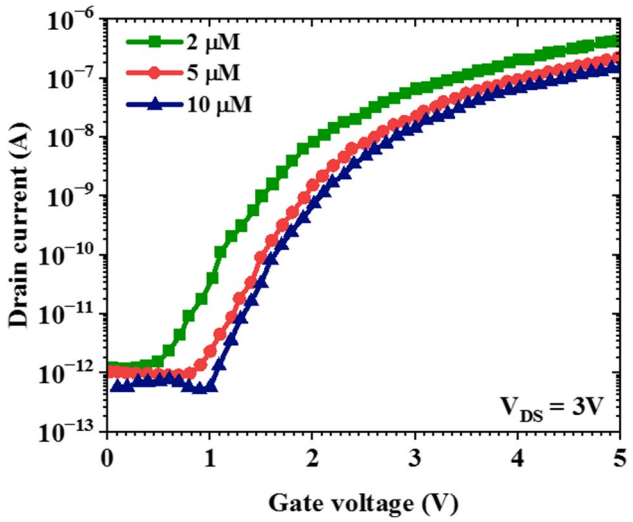

Fig. 8 Transfer characteristics plot of horn-like polycrystalline-SilNW FET biosensor for different channel length [46]

dengue virus DNA with enhanced sensitivity. Three step process namely surface modification of SilNW, immobilization of DNA and DNA hybridization was employed to make the device as a functional sensing element. It was suggested that altering the SilNW surface with oxygen plasma treatment would be an efficient way to increase the amount of target DNA binding. When compared to untreated SilNW device, oxygen plasma treated-SilNW device reported enhancement in current measurement. From the IV characteristics, improved efficiency was evident in SilNW device with 60 second of oxygen plasma treatment which will degrade after 90 second of treatment. 1.985 x 10^{-14} M detection limit was reported in plasma oxygen treated SilNW sensor with a linear range of detection 1.0 x 10^{-9} M to 1.0 x 10^{-13} M.

In 2016 K. Kim et al. [48] reported SilNW biosensor for label free recognition of biomarker cTn1-cardiac troponin-I. The nanowire configuration of the fabricated SilNW cardiac troponin biosensor utilized a honeycomb structure embedded with Ag/AgClpRE (Fig. 9) and exhibited enhanced electrical performance for various cardiac troponin-I concentration (Fig. 10) along with improved sensing area. The sensor reported n-type behaviour with less sub threshold swing, small leakage current at gate and high OFF-ON current ratio. The detection limit as low as 5 pg/mL, high sensitivity with low ion concentrations under buffer solutions along with excellent specificity for sensing cardiac troponin-I biomarker were also reported in the fabricated honeycomb SilNW biosensor. In the same year, M.Nuzaihan.M.N et al. [49] reported p-type molecular gate control based SilNW biosensor (Fig. 11) for sensing dengue virus related DNA. A three-step process that involved DNA immobilization, surface modification and hybridization were used to functionalize the surface of the fabricated SilNW. 45.0 μAM^{-1}sensitivity and 2.0 fM detection limit were reported in the fabricated p-type dengue virus SilNW biosensor.

In the year 2017, G. Presnova et al. [50] reported gold nanoparticles functionalized SilNW FET biosensor for label free and instantaneous detection of prostate specific antigen in human serum. The SilNW FET exhibited enhanced electrical performance and improved sensitivity to pH when

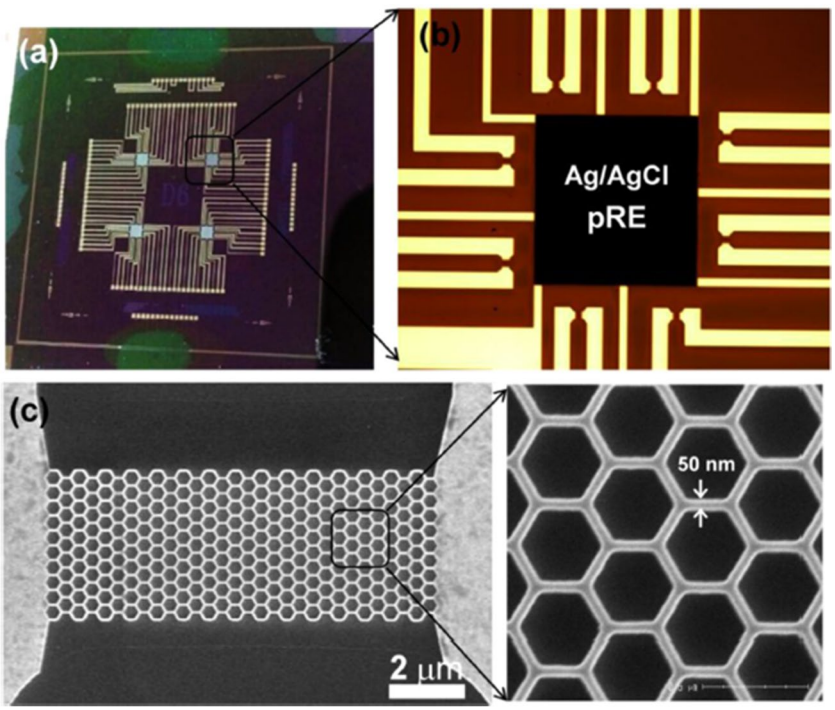

Fig. 9 (**a**) and (**b**) Optical images of SilNW honeycomb FET (**c**). Scanning electron microscopy image of SilNW honeycomb FET [48] (Copyright @ Elsevier)

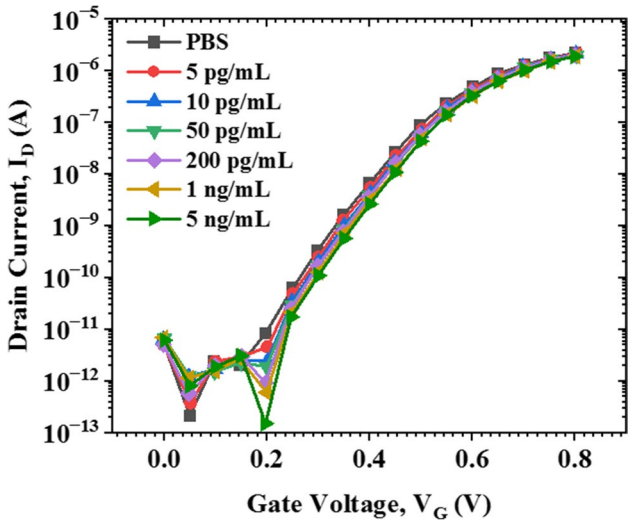

Fig. 10 V-I characteristics of honeycomb SilNW cardiac troponin-I biosensor [48]

the gold nanoparticles were used. The SilNW FET biosensor reported a response time of 5s to 10s and one minute analysis time per sample. 23 fg/mL detection limit and the prostate specific antigen detection range of 23 fg/mL to 500 ng/mL were also reported.

In the year 2018, B. L. Borgne et al. [51] reported three dimensional SilNW based resistor (Fig. 12) for real time sensing of Escherichia coli bacteria. Using gold as catalyst, vapour liquid solid process is used to synthesize SilNWs. Through electrical measurement, resistor exhibited Escherichia coli bacteria detection ability at lower concentration of 6×10^3 CFU/mL. In the year 2019, K. Zhou et al. [52] reported SilNW pH sensor fabricated using side wall mask technology via CMOS compatible process. Instead of using advanced lithography facilities, side wall mask technology facilitate in obtaining 10s or 100s of nano-meter feature sizes through film deposition method. This will help in the fabrication of SilNW with easy availability, low cost and high output. The sensor reported high sensitivity of 54.5 mV/pH, stability as well as repeatability in the pH range of 1 to 12. From the repeatability test measured for three times, 8 nA largest deviation was reported corresponding to 2.3%FS (Fig. 13).

In the year 2020, H. Zhang et al. [53] investigated the design as well as fabrication of SilNW biosensor through integration of critical factors for high sensitive detection of bio-molecules. Critical factors which affect the sensing performance of SilNW sensors namely functional interface, detection target and structure were analysed so as to enhance the sensing performance. It was reported that n-type narrow SilNWs with modest doping concentrations for impurities are useful for superior sensitive detection of negatively charged molecules. By controlling the thickness of the phosphorus dopant layer and thermal diffusion temperature, an n-type Sil layer with a doping concentration of $2x10^{16}$ cm^{-3} to $6x10^{16}$ cm^{-3} was synthesized. Through the use of controlled plasma etching and a high-resolution EBL method, high-quality SilNWs of 16.0 nm width were fabricated. In order to transport the trapped charged molecules near the SilNW surface, the layer of native oxide on SilNW was used as the gate-insulator. The SilNW width of 16 nm in the biosensor exhibited exceptional FET properties, demonstrating the biosensor's potential to recognise biomolecules in very low concentrations. Additionally, 2-aminoethylphosphonic

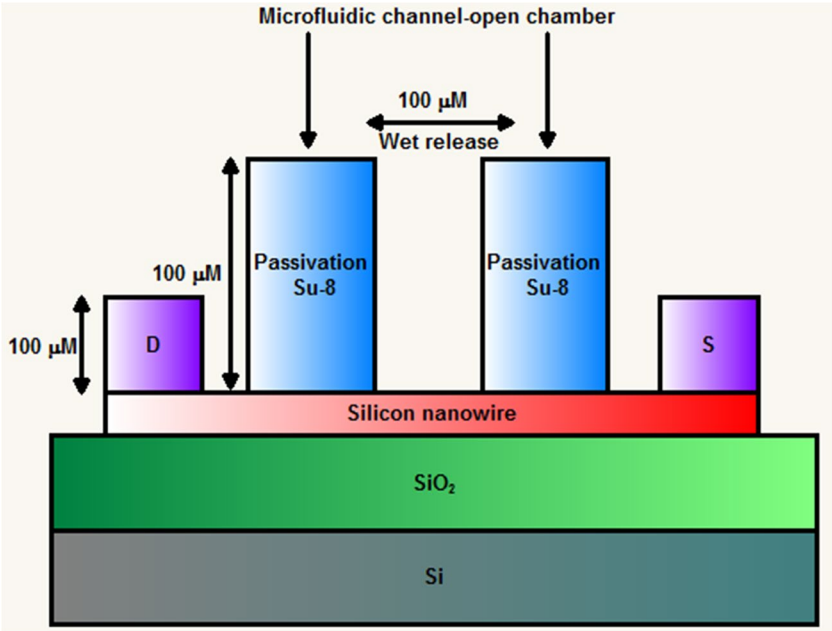

Fig. 11 Schematic illustration of SilNW integrated with microfluidic channel [49]

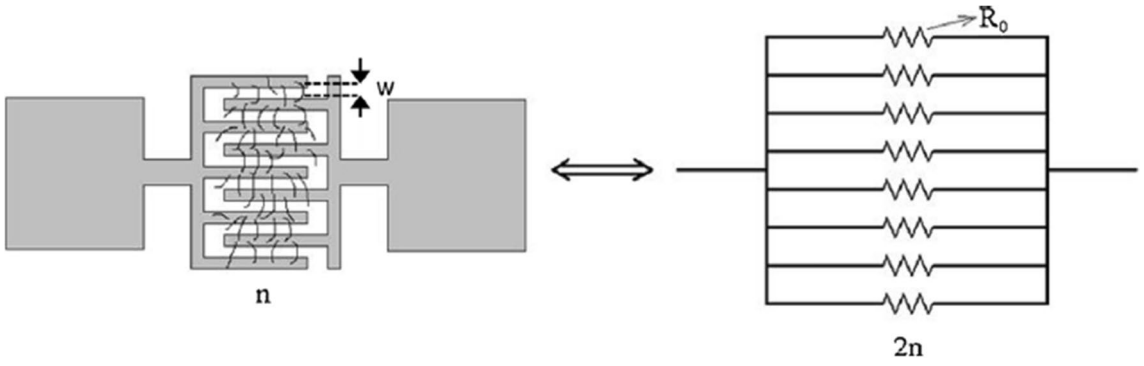

Fig. 12 Equivalent circuit diagram representation of SilNW resistor [51] (Copyright @ Elsevier)

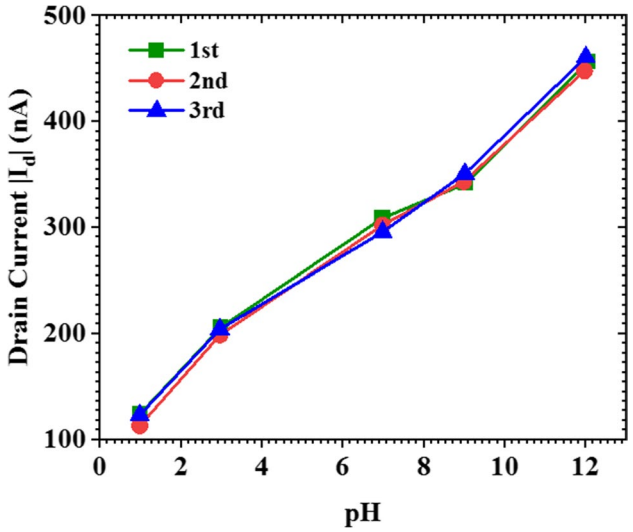

Fig. 13 SilNW pH sensor repeatability test measured for three times in the pH range of 1 to 12 [52]

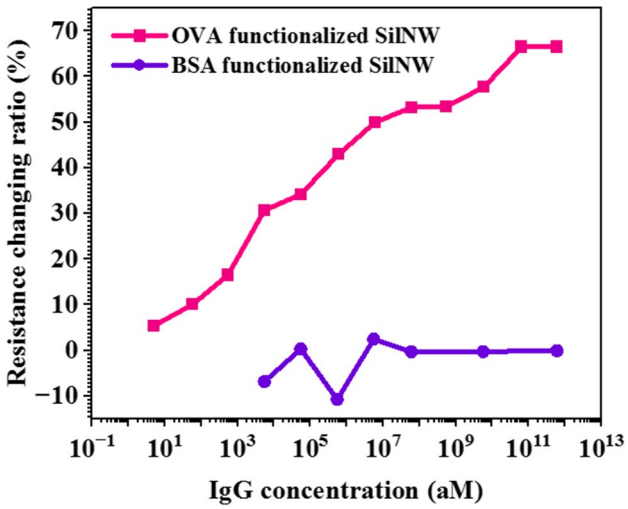

Fig. 14 Resistance changing ratio vs. IgG concentration plot of OVA functionalized and BSA functionalized SilNWs [53]

acid coupling was used to alter the SilNWs' surface, and SilNW surface was functionalized using OVA molecules for target IgG molecules capture and to detect IgG with high specificity (Fig. 14) and sensitivity. 6 aM detection limit and detection range of 6 aM to 600 nM was reported in the optimized SilNW biosensor towards target IgG.

In the same year, A. Gao et al.[54] reported B-nose based on AgOBP-functionalized SilNW array for sensing volatile odorant molecules emitted by human. On a commercial SOI (111) wafer, the SilNW array was fabricated using a low-cost novel top-down fabrication technique. With electric read-outs, the AgOBP-SilNW device exhibited repeatable and reversible response. Highly specific structural selectivity and excellent sensitivity down to 2 ppb were also reported by the B-nose device. In the year 2021, D. Li et al. [55] reported SilNW array biosensor for quantitating tumor marker circulating tumor DNA. The 120 SilNWs served as a molecular gate for identifying the target circulating tumor DNA after being silanized with the probe DNA. This SilNW-array FET biosensor exhibited remarkable selectivity in the recognition of complementary target circulating tumor DNA from one, two, or whole base mismatched DNA. The sensor reported 10 aM detection limit and a linear detection range of 0.1 fM to 100 pM. Additionally, SilNW array FET biosensor successfully identified target circulating tumor DNA in samples of human serum, indicating its promising future clinical application. In 2021, V. Gautam et al. [56] reported SilNW/reduced graphene oxide nano composite based biosensor for detecting biomarkers of infectious diseases formaldehyde and cyclohexane. MACE (metal-assisted chemical etching process) was used to fabricate SilNW, which at room temperature was then casted using graphene oxide. Under an inert atmosphere SilNW/graphene oxide was reduced to SilNW/reduced graphene oxide nano-composite using argon gas. SilNW/reduced graphene oxide nano-composite was characterized using scanning electron microscope, energy

dispersive spectrometer, transmission electron microscope, X-ray diffractometer, fourier transform infrared and Raman spectroscopy. At room temperature, the SilNW/reduced graphene oxide nanocomposite sensor exhibited a response of 1.07 and 0.99 for cyclohexane and formaldehyde concentrations of 1 ppm, respectively. The sensor displayed a quick response time of 30 s under ambient settings as well as detection limit of 1 ppm. The sensor also reported good repeatability (Fig. 15) and reproducibility. For cyclohexane and formaldehyde, the sensor's recovery time was 1-2 min and 3 min, respectively.

In the year 2022, Y. Benserhir et al. [57] reported fabrication of highly sensitive SilNW based Escherichia coli bacteria detection sensor. This research employs a method that quantitatively assesses the contribution of bacteria immobilized on nanowires sandwiched between two electrodes via measuring significant change in current. 83 μA CFU/mL per decade sensitivity due to nanometric dimensions of the nanowires and 10^2 CFU/mL limit of detection to various Escherichia coli concentrations along with linear detection range of 10^2 CFU/mL to 10^8 CFU/mL were reported. In the same year, W. Zhao et al. [58] reported SilNW FET biosensor device modified chemically with special antibodies for label free and electrical detection of exosomes. Using standard microelectronic process, the SilNW FET was fabricated with 45 nm width NWs and was packed in a polydimethylsiloxane microfluidic channel. Further specific CD63 antibody was used to modify nanowire to form SilNW FET biosensor. The sensor reported 2159 particles/mL limit of detection for A549 exosomes. SilNW FET biosensor also reported the ability to sense real time changes in exosomes. The sensor exhibited real time decrease in current with increase in exosome concentration. In the year 2023, J.E.Santana et al.

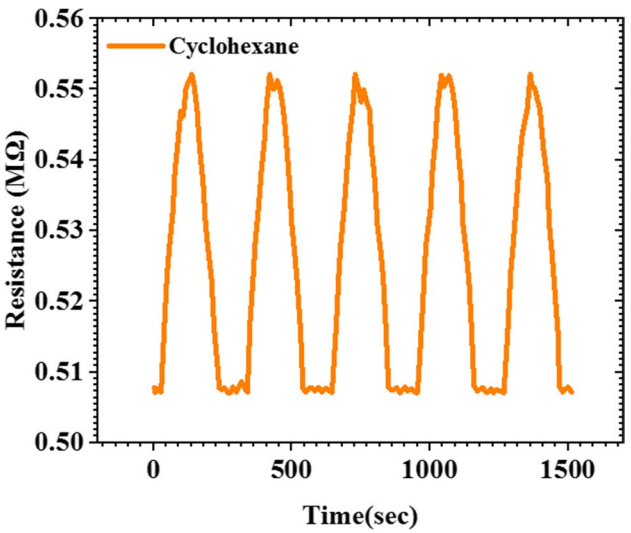

Fig. 15 SilNW/reduced graphene oxide biosensor repeatability for cyclohexane at 1 ppm concentration [56]

[59] investigated the effect of amphetamine adsorption on the electronic and structural properties as well as on the work function of pristine and modified SilNWs. Amphetamine which is one of the most commonly used illicit drug, was also employed in different medicinal therapies. Therefore, accurate tracking of amphetamine in various contexts is essential for its controlled distribution, even inside the human body. The two forms of changes that were investigated were surface functionalization using the same species as well as substitutional doping using boron, aluminium, and gallium atoms. Doped nanowires reported higher adsorption energies for the amphetamine molecule than functionalized ones and undoped SilNWs. It was also reported that Boron is the best chemical species for enhancing amphetamine adsorption for both doped and functionalized SilNWs. In the year 2023, J.E.Santana et al. [60] reported SilNW functionalized with copper, silver and gold transition metal atoms for selective sensing of RNA/DNA nucleobases. The adsorption of single RNA/DNA nucleobases cytosine, adenine, thymine, uracil and guanine was examined using Density Functional Theory first-principles computations. It was observed that guanine, adenine and cytosine were more favourably adsorbed by copper functionalized SilNWs and uracil and thymine prefer to adsorb on gold functionalized SilNWs. As a whole, nucleobase adsorption modifies the metal functionalized SilNWs original band structure by generating new localised states inside the band gap and close to the conduction band border which will enable their optical detection. The work function magnitude of the metal functionalized SilNW varies as a result of nucleobase adsorption. The copper functionalized SilNW exhibited the highest work function variation of 0.4 eV upon guanine and adenine adsorption. The sensing performance of different SilNW bio-sensors was given in Table 1 [31–93].

3 Silicon Nanowire Based Covid-19 Sensors

The covid-19 virus outbreak in the year 2019–2020 caused thousands of deaths and widespread fear across the globe. The covid-19 virus has a high rate of transmission and is deadly. In addition to being a health emergency, covid-19 created an adverse financial impact. In March 2020, covid-19 was declared a worldwide pandemic and health emergency. In terms of electrical detection, one of the most promising platforms for covid-19 virus is a biosensor based on semiconductor field-effect devices [94–98]. In 2022, A. Wasfi et al. [99] reported SilNW FET based covid-19 sensor using a semi-empirical modelling approach integrated with covid-19 anti-spike protein antibody. A. Wasfi et al. investigated the charge transport properties of SilNW FET which consists of a channel, gate and two electrodes. Significant changes in transmission spectra current, and conductance were seen

Table 1 Sensing performance and application of different SilNW biosensors [31–93]

Ref	SilNW sensor type	Target	LoD	Detection Range	Sensitivity	Response Time
[31]	Organophosphonate based PNA functionalized SilNW	DNA	-	-	-	-
[32]	SilNW sensor	Dengue virus	10 fM	-	-	30 minutes
[33]	Gold nanoparticle embedded SilNW biosensor	DNA	1 pM	-	-	-
[34]	Morpholino functionalized SilNW biosensor	DNA	100 pM	-	-	-
[35]	SilNW modified by gold NPs	Albumin	-	1 to 7μM	-	-
[36]	SAM-assisted SilNW biosensor	ERα	10 fM	-	-	-
[37]	SilNW array	DNA	-	-	-	-
[38]	SilNW FET biosensor	DNA-HMGB1 binding	-	-		
[39]	SilNW biosensor	DNA	-	-	-	-
[40]	N_2O plasma modified SilNW biosensor	Interleukin-1β gene	2.5 fM	-	0.12/decade	-
[41]	Modified SilNW sensor	Alkaline phosphatase	0.0175 U/mL	0.0175 to 0.3 U/mL	-	20 minutes
[43]	Multi-channel SilNW biosensor	Cardiac troponin I	320 fM	-	-	-
[44]	Liquid-based gate-control SilNW biosensor	ssDNA	0.1 nM	100 pM to 25 nM	-	-
[45]	SilNW/Amplifier MOSFET Hybrid biosensor	pH detection	-	-	-	-
[46]	SilNW -Polycrystalline FET biosensor	Ferritin	50 pg/mL	50 pg/mL to 500 ng/mL	133.47 mV/pH	-
[47]	O_2 plasma treated SilNW biosensor	Dengue Virus	1.985 x 10^{-14} M	1.0 x 10^{-9} M to 1.0 x 10^{-13} M	-	-
[48]	SilNW FET biosensor	Cardiac troponin I	~5 pg/mL	-	-	-
[49]	SilNW biosensor	Dengue virus DNA	2.0 fM	-	45.0 μAM^{-1}	-
[50]	SilNW FET biosensor	PSA	23 fg/mL	23 fg/mL to 500 ng/mL	70 mV/pH	5 to 10 seconds
[51]	3D SilNW based resistor	Escherichia coli bacteria	6×10^3 CFU/mL	-	-	< 1hour
[52]	SilNW FET	pH detection	-	-	54.5 mV/pH	-
[53]	n-type SilNW	IgG	6aM	6 aM - 600 nM	-	-
[54]	SilNW array	Volatile odorant molecules	-	-	-	-
[55]	SilNW array biosensor	ctDNA	10 aM	0.1 fM to 100 pM	-	-
[56]	rGO/SilNW nanocomposite	Cyclohexane and formaldehyde	1 ppm	-	-	30 seconds
[57]	SilNW biosensor	Escherichia coli bacteria	10^2 CFU/mL	-	83 μA/decade of CFU/mL	-
[58]	SilNW bio FET	Exosomes	2159 particles/mL	-	-	-
[59]	SilNW sensor	Amphetamine drug detection	-	-	-	-
[60]	Metal functionalized SilNW sensor	RNA/DNA nucleobases	-	-	-	-

Table 1 (continued)

Ref	SilNW sensor type	Target	LoD	Detection Range	Sensitivity	Response Time
[61]	SilNW FET	Cancer biomarker detection	-	-	-	-
[62]	SiNW-ECIS	Cancerous cultured living lung cells detection	-	-	-	-
[63]	SilNW FET	Particle counting	-	-	-	-
[64]	SilNWs/anti-PSA/AgNPs/MCH sensor	Prostate specific antigen	0.1 $\mu g.L^{-1}$	0.1-20 $\mu g.L^{-1}$	-	-
[65]	SilNW FET	MMP-9	7.6 pg/ml	-	86.96%	-
[66]	SilNW FET decorated with polyethylene glycol	MicroRNA	10 aM	10 aM to10 pM	-	-
[67]	SilNW FET	ALT	4.1 ± 0.4 U/L ALT	-	-	-
[68]	SilNW FET	pH	5nS/pH unit	-	-	-
[69]	SilNW ion sensitive FET	pH	-	-	-	-
[70]	Coaxial structured ZnO/SilNW EGFET	pH	-	-	46.25 mV/pH	-
[71]	SilNW dual gate sensor	pH	-	-	1438.8 mV/pH	-
[72]	Double gate SilNW FET	pH	-	-	720.7 mV/pH	-
[73]	SilNW with SiO_2/Al_2O_3 sensing membrane	pH	-	-	60.2 mV/pH	-
[74]	IGZO/SilNW sensor	pH	-	-	50 mV/pH	-
[75]	SilNW	Intracellular biochemical sensing	-	-	-	-
[76]	SilNW PDMS	Prostate specific antigen	1 fg/mL	-	-	-
[77]	SilNW FET	α-fetoprotein	-	500 fg/mL to 50 ng/mL	-	-
[77]	SilNW FET	Carcinoembryonic antigen	-	50 fg/mL to 10 ng/mL	-	-
[78]	SilNW array biosensor	Carcinoembryonic antigen	10 fg/mL	10 fg/mL to 100 pg/mL	-	-
[79]	SilNW FET	Carcino embryonic antigen	1 fg/ml	-	-	-
[79]	SilNW FET	microRNA 126	0.1 fM	-	-	-
[80]	Magnetic graphene composite modified poly-SilNW-FET	APOA2 protein	6.7pgmL^{-1}	19.5pgmL^{-1}-1.95µgmL^{-1}	-	-
[81]	Silicon on insulator nanowire biosensor	D-NFATc1 protein	10^{-15} M	-	10^{-14} M	-
[82]	SilNW FET	α-fetoprotein	10 ng/ml	-	-	-
[83]	SilNW FET	α-fucosidase	1.3 pM	-	-	-
[84]	SilNW FET	Vascular endothelial growth factor	2.59 nM	-	-	-
[85]	SilNW FET	ALCAM biomarker	15.5 pg/ml	-	-	30 minutes
[86]	SilNW FET	Vascular endothelial growth factor	-	5to 200 fM	-	-
[87]	SilNW FET	DNA	1 fM	-	-	-
[88]	SilNW FET	DNA	0.1 fM	-	-	-
[89]	Silicon on insulator NW biosensor	microRNA	10^{-17} M	-	-	-

Table 1 (continued)

Ref	SilNW sensor type	Target	LoD	Detection Range	Sensitivity	Response Time
[90]	Silicon on insulator nanowire biosensor	Tumor M2-PK	-	10^{-13} to 10^{-15} M	-	-
[91]	SilNW FET Sensor Arrays	CRP proteins	-	-	1.2 nA/dec	-
[92]	SilNW FET	H3N2 virus	10^4 viruses/L	-	-	-
[93]	SilNW sensor	Influenza A viruses	29 viruses/μL	-	-	-

in the presence of the covid-19 spike protein. The sensors performance was evaluated using the variation in current. The difference between bare sensors current and the current for the sensor as a result of the positioning of the target molecule was computed. The spike protein which is negatively charged caused extra hole-carriers, which decreased the current from drain of the SilNW-FET sensor during the placement of the target molecule (Fig. 16).

In the year 2022, B. Gao et al. [100] reported vertically oriented SilNW array based sensor for spike protein SARS-Covid-2 detection. Biosensor is based on vertically oriented SilNW arrays coupled to angiotensin converting enzyme-2, has strong selectivity and sensitivity for sensing SARS-Covid-2 spike protein. (Fig. 17). Using a metal-assisted chemical etching method, huge area arrays of vertically oriented SilNW arrays were created. The Sil substrate was transformed into a p-n junction diode that is electrically active following the vertical SilNW metal-assisted chemical etching process. The fabricated SilNW biosensor has 10^{10} vertical SilNWs per cm^2 area density and 350 nm average vertical SilNW length. 100 ng/ml limit of detection and response time of less than one hour have been reported in

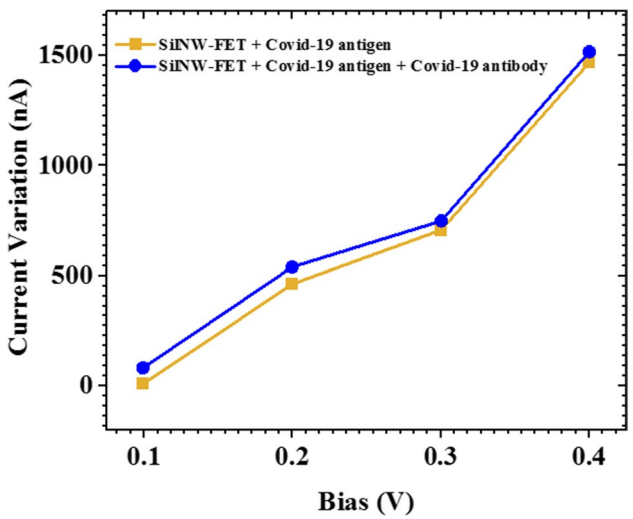

Fig. 16 Drain current variation in SilNW covid-19 sensor due to spike protein [99]

the fabricated vertical SilNW covid-19 biosensor. Offering a viable point-of-care detection approach for SARS-Covid-2 virus, the vertical SilNW sensor exhibited excellent specific response to the spike protein compared to negative controls.

In the year 2022, Chi-Chang Wu [101] reported polycrystalline SilNW FET sensor to detect SARS-Covid-2 spike protein. In order to keep the NW diameter within 100 nm, sidewall spacer etching was used to fabricate SilNW FET. 125 mV/decade sub-threshold swing and 10^6 on-off current ratio were reported in SilNW FET which indicates its strong stability and attributes. Using a pH range of 6 to 9 to evaluate solution, the polycrystalline SilNW FET biosensor exhibited a sensitivity of 59 mV pH^{-1}. The sensor also reported a limit of detection of 0.51 ag ml^{-1}.

4 Silicon Nanowire Based Gas Sensors

For the purpose of identifying different gases that have a harmful environmental impact as well as on people safety, gas sensors play a crucial role in our daily lives. Due of their distinct electrical characteristics, SilNWs finds application in instantaneous, sensitive and label-free detection of different gases. The SilNW based devices used for gas sensing are made up of both vertically standing and in-plane oriented SilNW [102–106]. In the year 2009, J. Wan et al. [107] reported SilNW sensor fabricated using PMMA/SiO_2/SU8 trilayer-nanoimprint method for gas detection. The SOI substrate, which is boron doped at $8x10^{17}$ cm^3 dopant concentration, was used in the fabrication of SilNW gas sensor. For comparison, a thin-film device and two SilNW sensors with 130 nm and 75 nm nanowire line widths were developed. The fabricated sensors were then used for sensing 250 ppm of NH_3 and NO_2. The carrier traps created during the reactive ion etching process after trilayer imprinting was reported as the reason for substantial increase in resistance of the NW devices. Due to its large surface to volume ratio, the narrower SilNW device in particular exhibited a notable improvement in sensitivity. 61.8% sensitivity for NH_2 gas and -19.7% sensitivity for NH_3 gas were reported in 75 nm SilNW sensor. In the year 2010, C. Gao et al. [108]

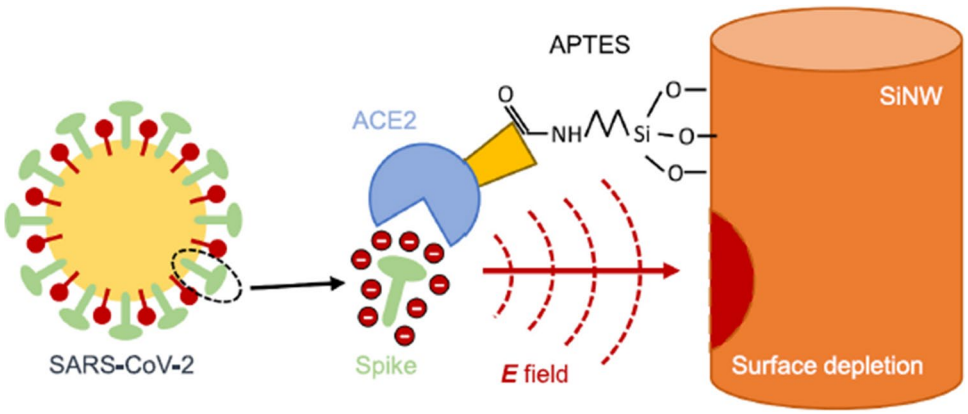

Fig. 17 Detection mechanism of vertically oriented SilNW biosensor [100] (Copyright @ Elsevier)

reported SilNW based gas sensor down to 22 nm wide fabricated using wet etching and trilayer nano imprint method. On the Sil on insulator substrate, samples with 22 and 75 nm top widths were developed. The fabricated devices were evaluated for NO_2 gas detection in a 250 ppm NO_2 environment. When compared to 75 nm wide one, 22 nm wide NW device reported higher relative sensitivity. Sensor with 22 nm NW width exhibited relative sensitivity of 14.7% for NO_2 while relative sensitivity of 7.0 % for NO_2 was reported in device with 75 nm NW width. In the same year, K. Skucha et al. [109] reported palladium/ SilNW schottky barrier FET based hydrogen sensor that functions at ambient temperature. The sensor was made of boron-doped contact-printed SilNW arrays on top of a Si/SiO_2 substrate with palladium contacts onto it that are subsequently evaporated. The sensor reported 6.9%/ppm sensitivity at 1000 ppm and was capable of reversibly and reliably detecting hydrogen concentrations in the range of 3 ppm to 5%. For hydrogen concentrations above 1000 ppm and over 100 ppm, the sensor reported a response that can be distinguished from noise and drift in less than 5 seconds and less than 30 seconds respectively. In the year 2011, C. Gao et al. [110] reported SilNW gas sensor fabricated via angled physical vapour deposition and bilayer nano imprint method with NW width ranging from 22 to 110 nm. This fabrication method was suggested as an alternate method for low-cost, high-resolution, ultra-thin and large-throughput production of NW sensors such that the widths of NW can be adjusted. On the boron-doped top Sil layers of the Sil on insulator substrate, SilNWs of varying widths were produced and was employed as the sensing components of gas sensor. The sensor with 60 nm SilNW width reported 155% sensitivity and SilNW with 90 nm width reported 44% sensitivity for 250 ppm of NO_2 gas. In the year 2013, L. Yang et al. [111] reported tellurium modified SilNW gas sensor for detecting propylamine and ammonia gas. Solution approach was used to grow tellurium nanoparticles on SilNWs, with an average diameter of 5 nm. Tellurium modified SilNW gas sensor exhibited low detection limits of 174 ppb and 196 ppb for propylamine and ammonia along with a detection range of 5 ppm to 25 ppm and 10 ppm to 400 ppm respectively. The sensor exhibited response time of 15 second and 5 seconds upon exposure to propylamine and ammonia. The recovery time reported was 6 second and 8 seconds respectively. The tiny size of tellurium nanoparticles has been ascribed as the reason for sensors quick response and high sensitivity. In the year 2014, Y. Wu et al. [112] reported p-porous Si/ p-TeO_2 NW gas sensor for detecting NO_2.Thermal evaporation was used to fabricate porous Si/ p-TeO_2 NW gas sensor using porous Sil as growth substrate and Te powder as the source material. At 26°C to 150°C working temperature (Fig. 18) and NO_2 concentrations that range from 0.05 ppm to 3 ppm, the gas sensing characteristics of pure porous Sil sensors and composite structure sensors were investigated. The composite structure sensor reported good NO_2 selectivity at room temperature, great repeatability and high responsiveness. In the year 2015, S. Naama et al. [113] reported SilNW based CO_2 gas sensor fabricated in $AgNO_3$/HF aqueous solution through metal-assisted one-step electroless etching technique. Platinum and gold nanoparticles were added to SilNWs via electroless metal deposition method.

Higher response was reported in gold modified structure biased with less voltages. The sensor response was computed as [113]

$$S = \frac{I_g - I_V}{I_V} \tag{4}$$

where I_v and I_g are the devices responsive current values in presence of primary vacuum and CO_2 gas.

In the year 2017, Y. Qin et al. [114] reported silver modified SilNW NH_3 gas sensor. Metal-assisted chemical etching was used to create SilNWs, and a key anisotropic post etching of TMAH was used to modify the silver NP in situ using the metal assisted chemical etching produced Ag dendrites. When compared to pristine SilNWs, approximately three

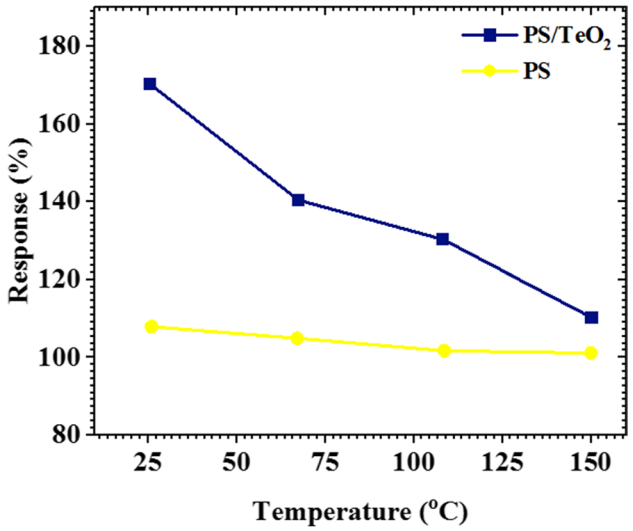

Fig. 18 Response curve to 1 ppm NO_2 of pristine PS and PS/TeO_2 NW gas sensor at various temperatures [112]

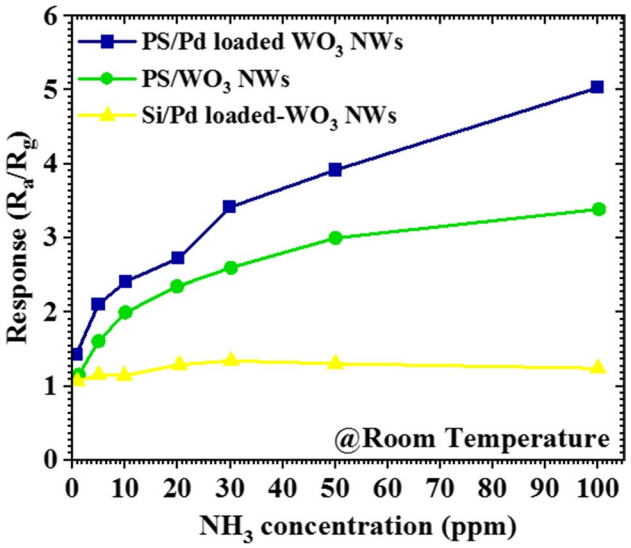

Fig. 19 Response of porous Sil/WO_3 NWs, porous Sil/Pd-loaded WO_3 NWs and Sil/Pd-loaded WO_3 NWs for various NH_3 concentrations in room temperature [116]

fold enhancement in gas response was reported in silver modified SilNWs. Response time, less than 2 seconds and recovery time less than 9 seconds were reported in silver modified SilNWs for 0.33 ppm to10 ppm of NH_3. In the same year, Y. Qin et al. [115] reported WO_3/SilNWs dendritic composite array based gas sensor for detection of NO_2. From the top section of each SilNW produced by metal-assisted chemical etching, WO_3 well-defined NWs form a hierarchical structure resembling dendrites. The WO_3/SilNWs exhibited response with significant improvement in NO_2 sensing. Exposure to 0.5 ppm to 5 ppm NO_2 resulted in transient response with response time less than 1 second. For the purpose of detecting ammonia at ambient temperature, sensitive porous Sil/Pd-loaded WO_3 NWs based resistive-type gas sensor was reported in the year 2018 by X. Qiang et al. [116]. Thermal evaporation of W powder over a porous Sil substrate was used to fabricate porous Sil/WO_3 NWs, and in-situ reduction was used to decorate the surface of the WO_3 NWs with Pd nanoparticles. The porous Sil/Pd-loaded WO_3 NWs exhibited a quick recovery-response time, strong selectivity, and an increased response to ammonia at low concentrations down to 1 ppm when compared to porous Sil/WO_3 NWs (Fig. 19). It was observed from the enhanced sensing properties that Pd NP was ideal in enhancing the performance of SilNW gas sensor.

In the year 2019, J. Yun et al. [117] reported high performance H_2 gas sensor with lower power usage and great stability against various environmental noises via suspended, self-heated and palladium decorated SilNWs. SilNWs were produced using standard complementary metal-oxide semiconductor technique, and palladium NPs were then added using a physical vapour deposition method to create the palladium decorated SilNWs. In contrast to existing palladium based H_2 gas sensors, joule heating of palladium-SilNW (< 1 mW) permits H_2 gas detection with a quicker response time and without a loss of sensitivity. In the year 2020, Y. Qin et al. [118] reported a stable clusters array of SilNWs with a special aggregation interconnection structure. The Cu_2O top-plating process used several spin-coatings of HF solution and Cu^{2+} on SilNWs to produce the stable aggregation interconnection structure. Vertical SilNWs with distinct tip aggregation interconnection structure in various clusters were produced by the top plating procedure in a stable and distinctive clusters array. The as-formed aggregation interconnection array was reported to be a highly efficient gas sensor, delivering a steady response with highly sensitivity and a low detection limit at ambient temperature. The aggregation interconnection-SilNWs sensor demonstrated a response value which is approximately 64 times better to 1 ppm NO_2 when compared to pristine SilNWs sensor. The sensor reported a limit detection of 5.4 ppb to NO_2 gas. In the year 2021, A. Mukherjee et al. [119] reported a high performance ultra-sensitive palladium nanoparticles decorated electrostatically formed SilNW based H_2 sensor. The electrostatically produced NW gate biases were properly tuned resulting in a sensitivity of approximately 400% ppm^{-1} and exceptional sensor response of $2x10^6$% for 0.8% H_2 (Fig. 20). The sensor also exhibited quick recovery and response times, strong sensing capability even with a relative humidity of 50%, and repeatability across time.

Ethanol is a vital VOC and significantly contributes to the detection of drunk driving. In the year 2021, Y. Qin et al. [120] reported SilNW ethanol sensor modified by ZIF-67 (Fig. 21) with enhanced moisture resistance and

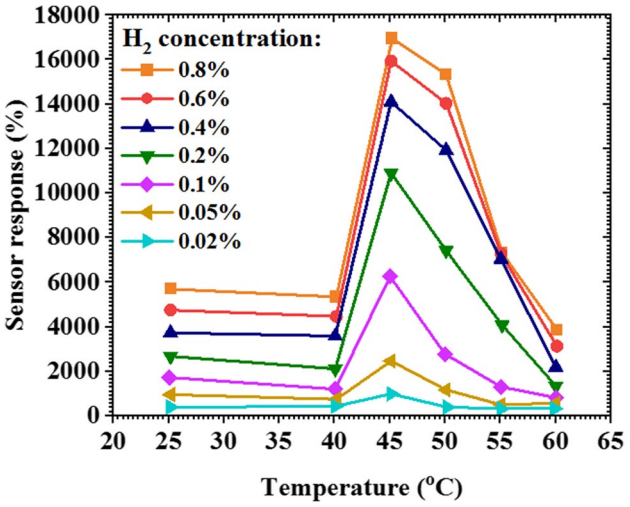

Fig. 20 Temperature vs sensor response plot of electrostatically formed SilNW sensor at various H_2 concentrations [119]

expanded detection range. The sensor showed a practical ability to detect 250 ppb ethanol with 25% response at room temperature with a 25% relative humidity. The developed ZIF-67 decorated SilNWs sensor still exhibited a substantial reaction when exposed to ethanol at concentrations between 0.25ppm to 200 ppm at high humidity of 65%. The sensor maintained 95% performance after 30 days and exhibited good concentration stability. In 2021, P. Dwivedi et al. [121] reported SilNW decorated with indium trioxide sensor for detection of ethanol. Metal assisted chemical etching method was used to fabricate SilNWs and thin film of indium was used to decorate it followed by annealing. Au-Cr inter-digitated electrode structure which was integrated on the top of the sensing layers was employed to compute the resistance change in order to measure the sensing response. At close to room temperature, the sensor's responsiveness to ethanol was greatly enhanced by indium trioxide integration in SilNWs. SilNWs and indium trioxide decorated SilNWs-based sensors reported 50 ppm and 10 ppm minimum ethanol detection respectively. The oxygen species present on indium trioxide NPs on the surface of SilNWs and the hetero structure generated at the interface was reported as the cause for this superior sensing behaviour. In 2021, X. Song et al. [122] reported integratable fabrication of SilNW based field effect sensors through in-plane step-guided solid-liquid-solid growth for ammonia gas sensing at room temperature. By tuning the back gated SilNW sensors into appropriate sub threshold detection regime, 75.8% excellent field-effect sensitivity at 100 ppm NH_3,100 ppb low limit of detection, rapid response/recovery time of 20 seconds and outstanding stability of over 180 days has been reported. These exceptional sensing abilities are due to the quick charge transfer between adsorbed NH_3 molecules and the exposed SilNW channels, suggesting a practical method for fabricating and deploying extremely effective gas detectors, which are in great demand in the emerging portable or wearable electronics market. The sensitivity of SilNW based field effect ammonia sensor was computed as [122]

$$S(\%) = \left[\left(\frac{|I_{ds}, NH_3|}{|I_{ds}, air|}\right) - 1\right] \times 100 \quad (5)$$

where $|I_{ds}$,air| and $|I_{ds}$,$NH_3|$ represents I_{ds} when exposed to air ambient gas and ammonia gas.

In the year 2022, V. Kashyap et al. [123] reported SilNW based nitrogen dioxide gas sensor fabricated through low cost metal assisted chemical etching technique.

The dislocation density of the synthesised SilNWs decreased concurrently with the rise in crystallite size, according to the structural study. The array of SilNWs had an approximate average size of 80 ± 0.001 nm and 97 ± 5 nm for the p_{40} and n_{40} samples respectively, according to the results of the morphological study. At 50 ppm, maximum sensing capabilities for the n_{40}-type SilNW based gas sensor was identified to be 68%, 63% and 35%

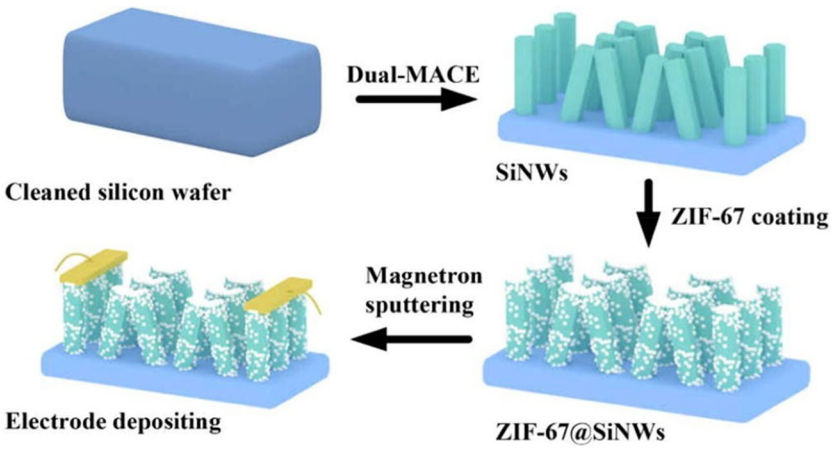

Fig. 21 Fabrication process of SilNWs decorated by ZIF-67 [120] (Copyright @ Elsevier)

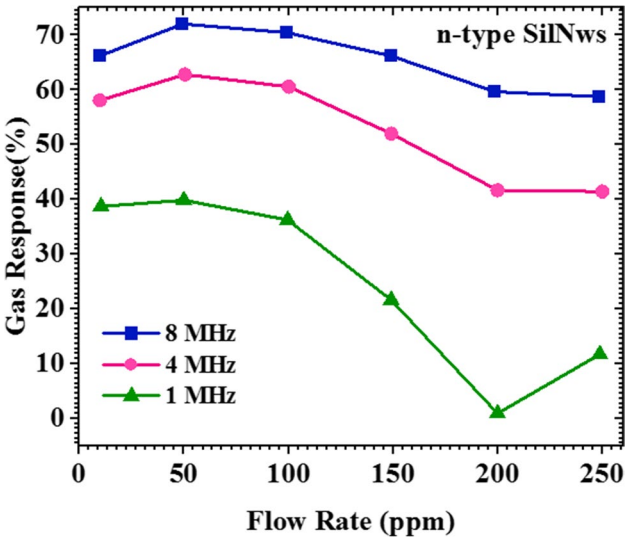

Fig. 22 n-type SilNW gas sensor response for different NO_2 concentration as a function of frequency [123]

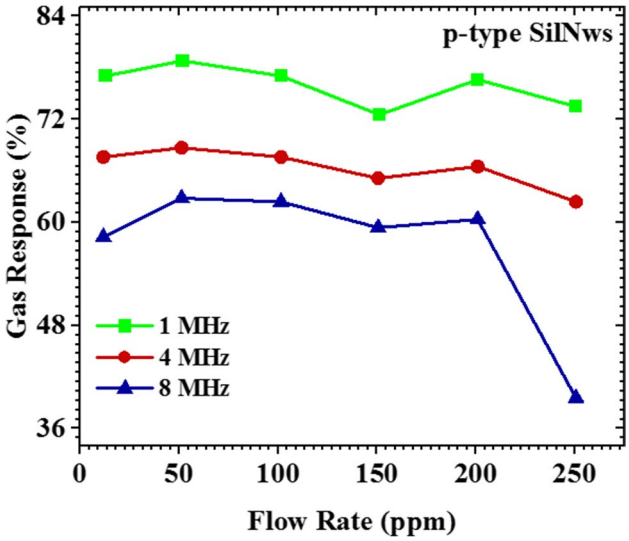

Fig. 23 p-type SilNW gas sensor response for different NO_2 concentration as a function of frequency [123]

at 8, 4, and 1 MHz, respectively, while it was 62%, 68% and 75% for the p_{40}-type SilNW based sensor. The results indicate that the n_{40}-type SilNW-based sensor is optimal in NO_2 gas detection at lower frequencies (Fig. 22) and room temperature, while the p_{40}-type SilNW-based sensor is ideal for NO_2 gas detection at room temperature and higher frequencies (Fig. 23).

In the year 2022, P. Nath et al. [124] reported SilNW ammonia sensor fabricated via metal assisted electrochemical etching process. On a Sil wafer that has been electroplated with silver, the etching process was carried out with the aid of dc-current delivered by an 6634B Agilent dc-power supply. The technique resulted in ordered SilNWs with a greater surface area. According to gas sensing tests, SilNWs exhibit reasonable recovery and response durations with 10 ppm low detection limit and are extremely selective for ammonia when compared to other gases, with improved response sensitivity. In the year 2023, R. Chaujar et al. [125] reported gate-all-around junctionless SilNW FET based hydrogen sensor. Palladium was used as a gate electrode because of its sensitivity to hydrogen gas. SiO_2 interface oxide and high dielectric oxide were used at the gate to combat electron tunnelling. Enhanced sensitivity was reported in gate-all-around junctionless SilNW FET hydrogen sensor when compared to bulk MOSFET and gate-all-around MOSFET. The results demonstrate that the gate-all-around junctionless SilNW FET based hydrogen sensor exhibited sensitivity improvements of 124.51% and 51.65%, respectively, over MOSFET and GAA-MOSFET, as 150mV palladium work function shifts at the gate. Sensing performance of different SilNW gas sensors was given in Table 2 [107–135].

5 Silicon Nanowire Based Chemical and Metal Ion Sensor

SilNWs were the focus of significant study for high sensitivity chemical sensors due to their surface potential sensitivity to charged species and their high surface to volume ratio [136–139]. In the year 2001, Y. Cui et al. [140] reported the first SilNW based chemical species sensor for streptavidin detection. SilNW modified with biotin were able to sense streptavidin in picomolar concentration range (10 pM). Y. Cui et al. also investigated the Ca^{2+} sensing of SilNWs which are crucial for triggering biological operations including contraction of muscles, cell death, protein release and cell development. The conductance decreased when a 25 µM Ca^{2+} solution was added, according to data obtained from modified SilNW devices, and then increased when a free buffer Ca^{2+} was subsequently passed through the device. Control trials using unaltered SilNWs showed no conductance change when Ca^{2+} was introduced, proving that the calmodulin receptor is necessary for detection.

Additionally, 10^{-5}M-10^{-6} M estimated dissociation constant, was compatible with the known K_d for calmodulin, and the observed conductance drop in modified SilNWs is consistent with predicted chemical gating by positive Ca^{2+}. Y. Cui et al. also investigated pH dependent conductance of oxide and amine functionalized SilNWs. The pH dependency was observed to be linear across the pH range of 2 to 9 (Fig. 24), making modified SilNWs ideal be used as pH sensors in the nanoscale. In the year 2008, X. Bi et al. [141] reported SilNW based electrochemical calcium sensor modified with phosphotyrosine. SilNWs were used as channels in a FET which is chemically gated

Table 2 Sensing performance of different SilNW gas sensors [107–135]

Ref	SilNW sensor type	Target	Sensitivity	LoD	Response Time	Recovery Time
[107]	Trilayer nano imprinted SilNW sensor (75 nm NW)	NH_2	61.8%	-	-	-
[107]	Trilayer nano imprinted SilNW sensor SilNW (75 nm NW)	NH_3	-19.7%	-	-	-
[108]	22 nm SilNW gas sensor	NO_2	14.7%	-	-	-
[109]	SilNW/Palladium schottky barrier based sensor	H_2	6.9%/ppm at 1000 ppm.	< 5 second for H_2 concentrations over 1000 ppm	-	-
[110]	Angle deposition +Bilayer NIL + RIE (60 nm SilNW)	NO_2	155% to 250 ppm NO_2	-	-	-
[111]	Tellurium modified SilNW	Ammonia	-	196 ppb	5seconds	8 seconds
[111]	Tellurium modified SilNW	Propylamine	-	174 ppb	15seconds	6 seconds
[112]	p-porous Si/p-TeO_2 NWs	NO_2	-	-	-	-
[113]	Au modified SilNW(0.5mbar)	CO_2	-	-	303 seconds	311 seconds
[113]	Pt modified SilNW(0.5mbar)	CO_2	-	-	143 seconds	120 seconds
[114]	Ag-modified SilNW	NH_3	-	-	≤ 2 seconds	≤ 9 seconds
[115]	SilNWs/WO_3 NWs	NO_2	-	-	< 1 seconds to 0.5ppm to 5ppm NO_2	-
[116]	Porous silicon/Pd-loaded WO_3 NWs	Ammonia	-	1 ppm	3 second - 10 second	-
[117]	Joule heated and suspended SilNW	H_2	-	-	-	-
[118]	SilNW arrays	NO_2	-	5.4 ppb	-	-
[119]	Palladium NPs decorated SilNW	H_2	~400 % ppm^{-1}	-	78 seconds	434 seconds
[120]	ZIF-67 modified SilNW	Ethanol	-	-	-	-
[121]	In_2O_3 decorated SilNW	Ethanol	-	10 ppm	-	-
[122]	Self-aligned SilNW FET	Ammonia	75.8% for100 ppm NH_3	100 ppb	-	-
[123]	Vertical SilNW array	NO_2	-	-	-	-
[124]	SilNW sensor	Ammonia	-	-	-	-
[125]	Gate-all-around junctionless SilNW FET	H_2	-	-	-	-
[126]	SilNW based resistor	NH_3 and Smoke	-	-	-	-
[127]	CuO NPs decorated SilNW	Non-enzymatic H_2O_2	22.27 μA/mM	1.6μM	-	-
[128]	Suspended SilNW	Ammonia	-	-	-	-
[129]	Bottom-gate SilNW FET	H_2	154.5%	-	-	-
[130]	SilNW/WO_3 NW	NO_2	-	-	-	-

Table 2 (continued)

Ref	SilNW sensor type	Target	Sensitivity	LoD	Response Time	Recovery Time
[131]	Si/tungsten oxide NWs	NO_2	-	-	14 seconds at 250°C	-
[132]	Vertically aligned SilNW/ZnO structures	CO_2	-	-	2 to 7 seconds	2 to 7 seconds
[133]	SilNW sensor	Petroleum vapor detection	-	-	-	-
[134]	MoS_2/porous SilNW	NO_2	-	1 ppm	-	-
[135]	SilNW/graphene heterostructure molecular sensors	H_2 and O_2	-	-	0.15/3.5 seconds	0.15/12 seconds

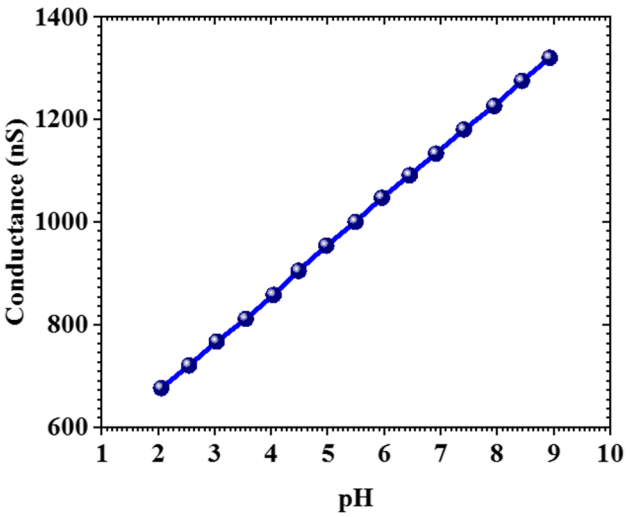

Fig. 24 Conductance vs. pH plot of oxide and amine functionalized SilNWs [140]

for the electrical detection of calcium ions. The SilNWs are modified with phosphotyrosine amino acid, which will bind the calcium ions with high affinity, to provide a sensitive and selective layer for calcium sensing. When exposed to aqueous solutions having calcium ions, phosphotyrosine modified SilNW reported increase in conductance with increase in concentration of calcium up to 10μM. In the same year, X. Bi et al. [142] reported SilNW FET sensor modified with tripeptide for detection of copper ions. Gly-Gly-His modified SilNWs was used as channel in the fabricated FET which reported excellent specificity and sensitivity to detect copper ions. The modified SilNW conductance change exhibits linear increase with logarithm of the copper concentrations and was attributed as the reason for stable complexation between Gly-Gly-His and copper ions. The percentage variation in conductance was computed as [142]

$$G\% = \frac{G_{Cu} - G_{buffer}}{G\_buffer} \times 100\% \quad (6)$$

where G_{buffer} and G_{Cu} represents Gly-Gly-His modified SilNW conductance without and with copper ions

Even in the presence of Zn, Gly-Gly-His modified SilNWs reported good selectivity and response for copper ions as low as 1 nM in real-time and with reversibility when compared to Gly-His-Gly-modified SilNWs. In the year 2009, X. Bi et al. [143] reported multi-channel ion sensor using oligopeptide modified SilNW arrays. Due to the top-down fabrication method used to create these SilNW arrays, very dense individually addressable SilNW (180 SilNWs organised into thirty six clusters) has been produced on a single chip. Sil-on-insulator wafers with Sil oxide and Sil that are each 50 nm and 80 nm thick, respectively, were employed as substrate. The concentrations of Cu^{2+} and Pb^{2+} in aqueous solutions may also be monitored concurrently and selectively in two separate channels after two distinct SilNW clusters have been modified with Cu^{2+} and Pb^{2+} selective oligopeptide respectively. 10 nM detection limit for Cu^{2+} and 1 nM detection limit for Pb^{2+} were reported in oligopeptide modified SilNW arrays. In the year 2011, J. Yin et al. [144] reported electro chemical hydrogen peroxide sensor based on SilNW arrays decorated with silver NPs. Silver ions can be reduced by the ordered H-terminated SilNW arrays fabricated by electroless etching, resulting in the deposition of silver NPs on SilNW. According to the electrochemical experiment results, the silver nanoparticles decorated SilNW array sensor showed more active areas for chemical reaction processes per unit area and high electrical conductibility. As a result, it has a quick amperometric sensing, a broad linear response spectrum, minimal detection limit and good sensitivity to hydrogen peroxide. The sensor can attain in 4 seconds, 95% of the maximum steady-state current at an applied voltage of 0.45V and a pH of 7.5 with 0.2 μM detection limit. In the year 2012, Q. Yan et al. [145] reported hydrogen peroxide sensor based on SilNW

modified with nickel hydroxide. The SilNWs/ nickel hydroxide electrode was made out of a nickel hydroxide coating layer that was applied using an electroless plating approach along with chemically etched SilNWs. By using amperometry and cyclic voltammetry, the analytical capabilities of the SilNWs/nickel hydroxide electrode for hydrogen peroxide measurement were examined. 3.31 mA mM^{-1} cm^{-2} sensitivity and 3.2 µm detection limit were reported in the fabricated SilNWs/ nickel hydroxide electrode based hydrogen peroxide sensor. In 2014, Y.M.Georgiev et al. [146] reported a highly precise junctionless SilNW biological and chemical sensing devices with a variety of shapes were made on SOI wafers using a top-down completely CMOS-compatible technique. Advanced PEC, high-resolution electron-beam lithography with the electron resist negative tone HSQ and RIE with CI-chemistry, were used for the patterning of the devices. A very high level of patterning quality was achieved in produced structures with little roughness between 0.8 nm and 1.6 nm and little variation in the SilNW widths from the intended values. When the devices were electrically characterised, junctionless back gated nanowire transistors with large on-currents in the range of 1µA to10 µA depending on the high ratios between the on-state and off-state currents of six-seven orders of magnitude and drain potentials were reported. In the same year, P. Livi et al. [147] reported a chemical sensor system having a chip with an array of SilNW ion sensitive FETs and CMOS readout. Each of the NWs has been interfaced to the CMOS circuitry, which consists of eight sigma-delta modulators and eight current-frequency converters, so as to apply a steady voltage for computing the corresponding current across each NW. Because each NW has its own exclusive readout channel, there is no need for multiplexing, which helps to prevent leakage current problems. In the year 2018, X. Cao et al. [148] reported SilNW based fluorescent facile sensor for dithionite detection. The sensor was fabricated by concurrently immobilising dabsyl group (recognising and quencher group) and dansyl group (fluorescent molecule) on the surface of SilNW and SilNW arrays. High selectivity and a strong linear connection between dithionite concentrations and fluorescence intensities between 0.1 mM and 1 mM were also reported. In the year 2021, Seong-Kun Cho et al. [149] reported sodium ion sensor based on SilNW dual gate FET. Extended gate sodium selective membrane was used as sensing unit and SilNW dual gate structured FET was used as transducer. For the SilNW pattern transfer, using electrospun polyvinylpyrrolidone nanofibers as a template, the Sil on insulator substrate was dry etched to create the SilNW channel dual gate FET. For NaCl solution, a sensitivity reading of 1464.66 mV/dec was recorded. The SilNW channel FET based sodium ion sensors outstanding selectivity was proved by the devices low sensitivities to buffer solutions including KCl, pH and $CaCl_2$.

In the year 2022, K. Daoudi et al. [150] reported hierarchical Ag nano prism/GO/SilNW arrays as raman scattering surface-enhanced sensors for atrazine detection (Fig. 25). Silver aided chemical etching has been used to successfully fabricate vertically and homogenous aligned SilNWs. Additionally, silver nano prism/GO/SilNW arrays were constructed by drop-casting the silver nano prisms after GO was spin-coated. In order to improve the homogeneous deposition of silver nano prisms, graphene oxide layers have been added to NW bunches. After graphene oxide modification, SERS characteristics significantly improved, with a SERS efficiency of $3.2x10^8$. The sensor reported 2.0×10^{-12} limit of detection for Atrazine. Sensing performance of different SilNW based Chemical and Metal Ion sensors was given in Table 3 [140–153].

6 Silicon Nanowire Based Various Other Sensors

SilNW has grown as an ideal material for sensing in various technological applications like temperature sensing, humidity sensing, pressure and strain sensing etc. In the year 2011, X. Chen et al. [154] reported humidity sensor based on SilNW. The SilNWs were modified using a monolayer self-assembled hexamethyldisilazane. Due to the methyl termination of the generated hexamethyldisilazane monolayer, the SilNWs surface becomes hydrophobic after modification. With its hydrophobic property, the sensors performance was reported to get enhanced by successfully preventing water vapour adsorption, enhancing charge storage stability and lowering surface conductivity. Humidity sensing behaviour of SilNWs based humidity sensors without and with hexamethyldisilazane modification was investigated. The hexamethyldisilazane modified SilNWs based humidity sensor shown enhanced humidity detecting behaviour, such as hysteresis, reaction time and linearity, compared to the SilNWs based sensor, due to the hydrophobic feature of hexamethyldisilazane. In the year 2012, H.Y.Wang et al. [155] investigated the capacitive humidity sensing characteristics of Sil carbide NW. On a nanoporous Sil pillar array, a catalyst-assisted chemical vapour deposition process was used to generate a significant number of entangled Sil carbide NW with 15 nm average diameter. By evaporating interdigital coplanar silver electrodes onto the surface of Sil carbide NW/Sil nanoporous pillar array, the capacitive humidity sensing capability at room temperature were investigated. At 100 Hz measurement frequency, a capacitance increase of nearly 960% was attained with a change in relative humidity from 11% to 95% (Fig. 26). At 75% relative humidity, the 4.5% maximum humidity hysteresis was measured and the response and recovery durations were recorded to be 105 seconds and 85 seconds respectively.

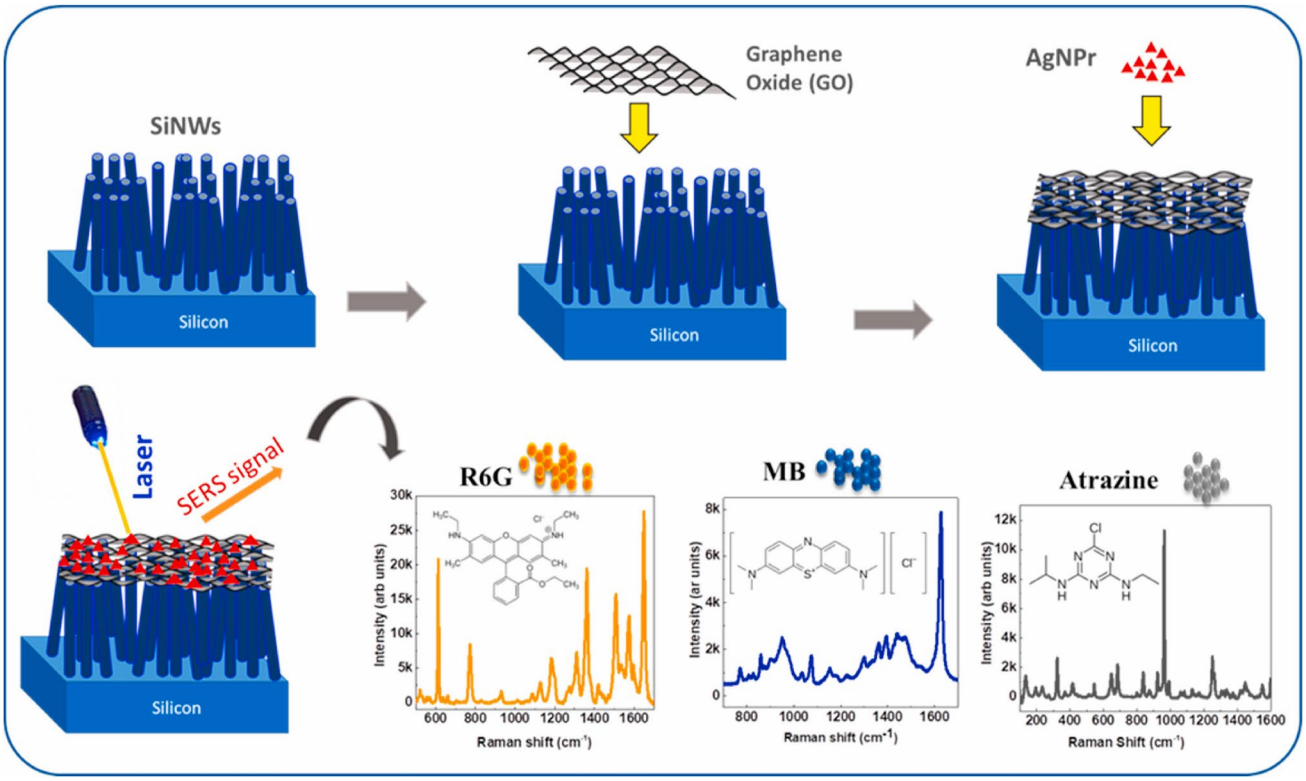

Fig. 25 Schematic representation of Ag nano prism/GO/SilNW chemical sensor [150] (Copyright @ Elsevier)

Table 3 Sensing performance of different SilNW based Chemical and Metal Ion sensors [140–153]

Ref	SilNW sensor type	Target	Sensitivity	LoD	Range of Detection
[140]	Biotin-modified SilNW	Streptavidin	-	10 pM	-
[141]	SilNW modified with p-Tyr	Calcium ions	-	1.2 nM	100 nM to 1 mM
[142]	Tripeptide modified SilNW FET	Copper ions	-	1 nM	-
[143]	Oligopeptide modified SilNW arrays	Pb^{2+}	-	1nM	-
[143]	Oligopeptide modified SilNW arrays	Cu^{2+}	-	10 nM	-
[144]	Silver nanoparticles decorated SilNW	Hydrogen peroxide	57.5 $\mu A mM^{-1} cm^{-2}$	0.2 µM	0.2 mM – 20 mM
[145]	Nickel hydroxide modified SilNW	Hydrogen peroxide	3.31 mA $mM^{-1} cm^{-2}$	-	-
[148]	Fluorescent SilNW sensor	Dithionite	-	-	0.1 to 1 mM
[149]	SilNW dual gate FET	Sodium ion	1464.66 mV/dec	-	-
[150]	Silver/GO/SilNW array	Atrazine	-	2.0×10^{-12} M	-
[151]	MPTES functionalized SilNW	Cd^{2+}	10^{-4}M	-	-
[151]	MPTES functionalized SilNW	Hg^{2+}	10^{-7}M	-	-
[152]	SilNW modified with R6G derivatives	Cu(II)	-	-	0.0 to 7.0 µM
[153]	SilNW FET	Organophosphorus molecules	-	-	-

A high degree of measurement repeatability and long-term stability were also demonstrated for the humidity sensor. In the year 2013, H. Taghinejad et al. [156] reported humidity sensor based on doped SilNW. Vapor-liquid-solid method was been used to fabricate SilNWs. Doping of NWs resulted in a noticeable increase in the device sensitivity. In the year 2014, S. Zhang et al. [157] reported a SilNW based novel piezo-resistor pressure sensor with an annularly grooved diaphragm. The advantage of the groove structure, which makes the stress to be localised in the rib area and results in a higher resistance change, was observed by both measurement and FEM data. The device's sensitivity was boosted by 2.5 times in pressure ranges of zero to120 mmHg compared to flat diaphragm pressure sensor. The sensor reported

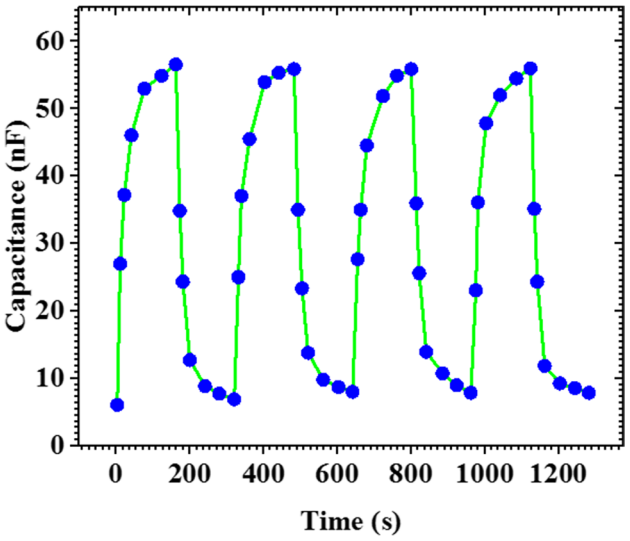

Fig. 26 Silicon carbide NW/Sil nanoporous pillar array time response curve by varying the ambient relative humidity between 11% & 95% at a frequency of 100 Hz [155]

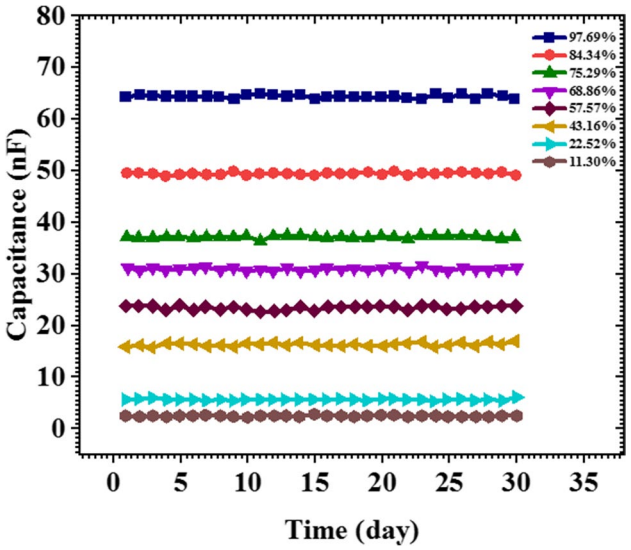

Fig. 27 Stability of ZnO nanorods/SilNW humidity sensor at room temperature for one month [158]

a sensitivity of approximately 8.92 x 10^{-5} (ΔR/R)/mmHg. In the year 2015, Z. Wang et al. [158] reported humidity sensor (capacitive) based on SilNW arrays with ZnO nanorods grown on it. Chemical bath deposition and wet chemical etching, respectively, were used to fabricate SilNWs with a length of about eight µm and zinc oxide nanorods with a length of about two hundred nm. When the relative humidity varies from 11.30% to 97.69%, the sensors maximum response range reported was 2.40 nF to 64.40 nF. The longest recovery and response time of seven seconds and twenty six seconds for 97.69% relative humidity was reported in the fabricated ZnO nanorods/SilNW humidity sensor along with a sensitivity of 0.69 nF/% RH. The sensors have 2.93% maximum relative standard deviation which corresponds to 11.30% relative humidity over the course of nearly a month at room temperature in air, demonstrating their long-term stability (Fig. 27).

In the year 2019, G. Chen et al. [159] reported highly self-assembling CMOS fabricated porphyrin-Sil hybrid NW transistor based photonic sensor. The selective assembly of a large number of porphyrin molecules to the surface of poly-SilNW was accomplished by carefully constructing the hydrophobic isolation structure in the device, which was confirmed by the AFM, SEM, and laser confocal fluorescence microscopy. Selective-assembling porphyrin-SilNW FET reported significantly greater photo-electronic detection sensitivity than classical devices, even at extremely low illumination power densities of 11.2 µW/cm^2. In the year 2020, C. Kim et al. [160] reported a SilNW based pressure sensor fabricated via metal assisted chemical etching process. In order to provide the sensor the necessary flexibility and high-pressure resistance, polydimethylsiloxane was applied to metal assisted chemical etched NWs, which had a height of 30 m and a diameter as tiny as 200 nm. As the applied pressure changes from 0 - 4.5 kPa, the piezo-resistance SilNW sensor reported a quick recovery and response time of 0.3 seconds, and it can differentiate pressure fluctuations as low as 0.3 kPa, which is far lower than the range that human skin can perceive (10 to 40 kPa). In the year 2021, J. Rhee et al. [161] reported SilNW based optical under display proximity sensor. Due to its strong photo-responsivity, SilNW can sense distance even when positioned underneath displays without using a significant amount of current for driver operation. Additionally, the read-out integrated circuit in the reported optical proximity sensor will eliminate the dark leakage current produced by SilNWs. The read-out integrated circuit takes up 0.18 mm^2 of space and the proximity sensor is made using a 0.18 µm CMOS technology. The optical proximity sensor can identify an item that is closer than 40 mm in each of the three scenarios with vertical cavity surface emitting laser generating currents of 12 mA, 10 mA and 7 mA. In the year 2022, Y. Yang et al. [162] reported strain sensor fabricated via two-step technique, including water-induced swelling and silver NW deposition, to create stretchable sensors with hierarchical wrinkled architectures. Sodium chloride particles were introduced into the elastomer matrix as highly soluble additives. The elastomer substrate experienced substantial swelling after being soaked in dopamine aqueous solution. The swelling process that occurs along with the dopamine deposition gives the sample surface ultra-hydrophilicity. When exposed to external deformation ranging from 10% to 100% stresses, the sensor exhibited great sensitivity, strong

Table 4 Sensing performance and applications of various other SilNW based sensors [154–171]

Ref	SilNW sensor type	Application	Sensitivity	Response Time	Recovery Time
[154]	Hexamethyldisilazane modified SilNWs	Humidity sensing	-	-	-
[155]	SiC NW/silicon nanoporous pillar array	Humidity sensing	-	105 seconds	85 seconds
[156]	Doped SilNW	Humidity sensing	-	-	-
[157]	SilNW	Pressure sensing	8.92 x 10^{-5} (ΔR/R)/mmHg	-	-
[158]	ZnO nanorods/SilNWs	Humidity sensing	0.69 nF/% RH	26 seconds	7 seconds
[159]	Porphyrinorphyrin-SilNW FET	Photonic Sensor	-	-	-
[160]	SilNW array	Pressure sensing	-	0.3 seconds	0.3 seconds
[161]	SilNW	Proximity sensor	-	-	-
[162]	SilNW with hierarchical wrinkled structures	Strain sensor	-	-	-
[163]	NEMS piezoresistive SilNW	Pressure sensing	0.42% psi^{-1}	-	-
[164]	SilNW array	Humidity sensing	-	-	-
[165]	SilNW	Hydrogen ion sensing	-	-	-
[166]	SilNW based NEMS sensor	Pressure sensing	-	-	-
[167]	SilNW	Optical rectangular waveguide sensor	-	-	-
[168]	SilNW	RFID Humidity Tag Sensor	-	-	-
[169]	High Anisotropy SilNW	Photonic Sensor	-	-	-
[170]	SilNW	Environmental air quality monitoring	-	-	-
[171]	SilNW	Pressure sensing	8.2 kPa^{-1}	3 milliseconds	-

electrical repeatability over 8000 stretch/release cycles, and consistent electrical response at various stretch/release frequencies.

The recent advancements in SilNW devices enable rapid and sensitive analysis in different prospective applications. It is expected that these enhanced sensing devices would be commercially produced and widely employed in our daily lives. Other than for sensing applications, in the last decade, significant advancements had also happened in the use of SilNWs for thermoelectric, photovoltaic, photo electrochemical power generation, energy storage with LIB anodes, photo detection etc. Sensing performance and applications of various other SilNW based sensors was given in Table 4 [154–171].

7 Conclusion

The rapid rise and development of sophisticated nanotechnology has led to the fabrication of several sensing nano materials with specific features, desirable sizes, and chemical compositions. The development SilNW technology will be considered as a very useful augmentation to the present Sil technology. The exceptional physical and chemical capabilities of SilNWs made them a good alternative for a variety of uses that depends on their extraordinary physicochemical qualities. The distinctive properties of SilNW sensor, such as biocompatibility, adjustable optical and electrical characteristics, and outstanding surface-to-volume ratio, make them a viable choice in the detection of various nucleic acids, viruses, chemicals, metal ions species and gases. However in order ensure the dependability of electrical and electrochemical SilNW sensors, the two broad manufacturing procedures of SilNWs must be developed more effectively. In the promising field of various sensing devices, Sil nanostructures will open way for more networked, smarter and portable platforms.

Author contributions Dr. S. Sreejith, Dr. J Ajayan and Dr. N.V. Uma Reddy have role in Conceptualization, Methodology, Writing Original Draft, Validation and Investigation. Dr. M. Manikandan have the credits to Software, Formal analysis, Resources, Data Curation, Writing Review and Editing.

Data availability Not applicable.

Declarations

Ethics Approval and Consent to Participate All procedures performed in studies were in accordance with the ethical standards of the institutional and/or national research committee and with the comparable ethical standards.

For this type of study, formal consent is not required.

Consent for Publication Authors give consent for the publication of the Submitted Research article in Silicon.

Competing interests The authors declare no competing interests.

Research Involving Human Participants and/or Animals Not Applicable.

Informed Consent Not Applicable.

Conflicts of Interest The authors declare that there is no conflict of interest reported in this paper.

References

1. Sreejith S, Ajayan J, Kollem S, Sivasankari B (2022) A comprehensive review on thin film amorphous silicon solar cells. Silicon 14:8277–8293
2. Sreejith S, Ajayan J, Radhika JM, Sivasankari B, Tayal S, Saravanan M (2023) A comprehensive review on graphene FET biosensors and their emerging application in DNA/RNA sensing & rapid Covid-19 detection. Measurement 206:112202
3. Cazimajou T, Mouis M, Legallais M, Nguyen TTT, Ternon C, Salem B, Ghibaudo G (2020) Analysis of the role of inter-nanowire junctions on current percolation effects in silicon nanonet field-effect transistors. Solid State Electronics 168:107725
4. Mishra SM, Dey S, Singha T, Mandal S, Dehury AK, Chaudhary YS, Satpati B (2023) Enhanced optical properties and dark I-V characteristics of silicon nanowire-carbon quantum dots heterostructures. Mater Res Bull 164:112262
5. Sreejith S, Joseph LMIL, Kollem S, Vijumon VT, Ajayan J (2023) Biodegradable sensors: a comprehensive review. Measurement 219:113261
6. Sreejith S, Ajayan J, Devasenapati SB, Sivasankari B, Tayal S (2023) Critical review on reliability and short circuit robustness of silicon carbide power MOSFETs. Silicon 15:623–637
7. Chen S, van den Berg A, Carlen ET (2015) Sensitivity and detection limit analysis of silicon nanowire bio(chemical) sensors. Sensors Actuators B 209:486–489
8. Hasheminia F, Bahari Y, Rajabpour A, Arabha S (2021) Elucidation of thermo-mechanical properties of silicon nanowires from a molecular dynamics perspective. Comput Mater Sci 200:110821
9. Mirsian S, Khodadadian A, Hedayati M, Manzour-ol-Ajdad A, Kalantarinejad R, Heitzinger C (2019) A new method for selective functionalization of silicon nanowire sensors and Bayesian inversion for its parameters. Biosens Bioelectron 142:111527
10. Gonchar KA, Moiseev DV, Bozhev IV, Osminkina LA (2021) Influence of H_2O_2 concentration on the structural and photoluminescent properties of porous silicon nanowires fabricated by metal-assisted chemical etching. Mater Sci Semicond Process 125:105644
11. Mussabek G, Lysenko V, Yermukhamed D, Sivakov V, Timoshenko VY (2020) Thermally induced evolution of the structure and optical properties of silicon nanowires. Results in Physics 18:103258
12. Yang R-r, Song C-k, Chen Y-j, Zeng G-w, Wang J-x, Chen J-h, Zhang W-c (2021) Silicon nanowire-based energetic materials with significantly improved hygroscopicity, energetic materials. Frontiers 2:105–110
13. Rashid JIA, Abdullah J, Yusof NA, Hajian R (2013) The development of silicon nanowire as sensing material and its applications. J Nanomater 2013:328093
14. Yu Y, Chen S, Hu Q, Solomon P, Zhang Z (2021) Ultra-low noise Schottky junction tri-gate silicon nanowire FET on bonded silicon-on-insulator substrate. IEEE Electron Device Lett 42:469–472
15. Fobelets K, Meghani M, Li C (2014) Influence of minority carrier gas donors on low-frequency noise in silicon nanowires. IEEE Trans Nanotechnol 13:1176–1180
16. Agarwal A, Buddharaju K, Lao IK, Singh N, Balasubramanian N, Kwong DL (2008) Silicon nanowire sensor array using top–down CMOS technology. Sensors Actuators A 145–146:207–213
17. Toan NV, Ito K, Tuoi TTK, Toda M, Po-Hung Chen MFM, Sabri J, Li TO (2022) Micro-heat sink based on silicon nanowires formed by metal-assisted chemical etching for heat dissipation enhancement to improve performance of micro-thermoelectric generator. Energy Convers Manag 267:115923
18. Tsuchiya T, Hemmi T, Jun-ya Suzuki Y, Hirai OT (2016) Tensile fracture of integrated single-crystal silicon nanowire using MEMS electrostatic testing device. Procedia Structural Integrity 2:1405–1412
19. Pakzad SZ, Esfahani MN, Alaca BE (2023) The role of native oxide on the mechanical behavior of silicon nanowires. Mat Today Comm 34:105002
20. Shalabny A, Buonocore F, Celino M, Zhang L, Sardashti K, Härth M, Schubert DW, Bashouti MY (2022) Enhancing the electronic properties of VLS-grown silicon nanowires by surface charge transfer. Appl Surf Sci 599:153957
21. Mazzetta I, Rigoni F, Irrera F, Riello P, Quaranta S, Latini A, Palma F (2021) Large-scale CMOS-compatible process for silicon nanowires growth and BC8 phase formation. Solid State Electron 186:108093
22. Adhila TK, Elangovan H, Chattopadhyay K, Barshilia HC (2021) Kinked silicon nanowires prepared by two-step MACE process: synthesis strategies and luminescent properties. Mater Res Bull 140:111308
23. Ray U, Sarkar S, Banerjee D (2022) Silicon nanowires as an efficient material for hydrogen evolution through catalysis: a review, Catal Today. https://doi.org/10.1016/j.cattod.2022.11.025
24. Gebavi H, Ristic D, Baran N, Marcius M, Gasparic V, Syed K, Ivanda M (2021) Development of silicon nanowires based on Ag-au metal alloy seedsystem for sensing technologies. Sensors Actuators A 331:112931
25. Ghiass MA, Armini S, Carli M, Caro AM, Cherman V, Ogi J, Oda S, Moktadir Z, Tsuchiya Y, Mizuta H (2011) Temperature insensitive conductance detection with surface-functionalised silicon nanowire sensors. Microelectron Eng 88:1753–1756
26. Zhang G-J, Ning Y (2012) Silicon nanowire biosensor and its applications in disease diagnostics: a review. Anal Chim Acta 749:1–15
27. Grieshaber D, MacKenzie R, Voros J, Reimhult E (2008) Electrochemical biosensors - sensor principles and architectures. Sensors 8:1400–1458
28. Namdari P, Daraee H, Eatemadi A (2016) Recent advances in silicon nanowire biosensors: synthesis methods. Propert, Appl, Nanoscale Res Lett 11:406
29. Shen M-Y, Li B-R, Li Y-K (2014) Silicon nanowire field-effect-transistor based biosensors: from sensitive to ultra-sensitive. Biosens Bioelectron 60:101–111
30. Ivanov YD, Romanova TS, Malsagova KA, Pleshakova TO, Archakov AI (2021) Use of silicon nanowire sensors for early cancer diagnosis. Molecules 26:3734
31. Cattani-Scholz A, Pedone D, Dubey M, Neppl S, Nickel B, Feulner P, Schwartz J, Abstreiter G, Tornow M (2008) Organophosphonate-based PNA functionalization of silicon nanowires for label-free DNA detection. ACS Nano 2:1653–1660
32. Guo-Jun Zhang L, Zhang MJ, Huang ZHH, Luo GKIT, Lim E-JA, Kang TG, Chen Y (2010) Silicon nanowire biosensor for highly sensitive and rapid detection of dengue virus. Sensors Actuators B 146:138–144
33. Ryu S-W, Kim C-H, Han J-W, Kim C-J, Jung C (2010) Hyun Gyu Park, Yang-Kyu Choi, gold nanoparticle embedded silicon

nanowire biosensor for applications of label-free DNA detection. Biosens Bioelectron 25:2182–2185
34. Guo-Jun Zhang ZHH, Luo MJ, Huang GKIT, Lim E-JA (2010) Morpholino-functionalized silicon nanowire biosensor for sequence-specific label-free detection of DNA. Biosens Bioelectron 25:2447–2453
35. Kwon DH, An HH, Hee-Soo Kim JH, Lee SH, Suh YH, Kim CSY (2011) Electrochemical albumin sensing based on silicon nanowires modified by gold nanoparticles. Appl Surf Sci 257:4650–4654
36. Zhang G-J, Huang MJ, Ang J'AJ, Liu ET, Desai KV (2011) Self-assembled monolayer-assisted silicon nanowire biosensor for detection of protein–DNA interactions in nuclear extracts from breast cancer cell. Biosens Bioelectron 26:3233–3239
37. Kulkarni A, Xu Y, Ahn C, Amin R, Park SH, Kim T, Lee M (2012) The label free DNA sensor using a silicon nanowire array. J Biotechnol 160:91–96
38. Duan X, Li Y, Rajan NK, Routenberg DA, Modis Y, Reed MA (2012) Quantification of the affinities and kinetics of protein interactions using silicon nanowire biosensors. Nat Nanotechnol 7:401–407
39. Serre P, Ternon C, Stambouli V, Periwal P, Baron T (2013) Fabrication of silicon nanowire networks for biological sensing. Sensors Actuators B 182:390–395
40. Jia-Yo W, Tseng C-L, Yang-Kao Wang YY (2013) Keng-Liang Ou, Chi-Chang Wu, detecting interleukin-1β genes using a N_2O plasma modified silicon nanowire biosensor. J Exp Clin Med 5:12–16
41. Wang H, Mu L, She G, Xu H, Shi W (2014) Fluorescent biosensor for alkaline phosphatase based on fluorescein derivatives modified silicon nanowires. Sensors Actuators B 203:774–781
42. Jayakumar G, Asadollahi A, Hellström P-E, Garidis K, Östling M (2014) Silicon nanowires integrated with CMOS circuits for biosensing application. Solid State Electron 98:26–31
43. Shen S-H, Wang I-S, Cheng H, Lin C-T (2015) An enhancement of high-k/oxide stacked dielectric structure forsilicon-based multi-nanowire biosensor in cardiac troponin I detection. Sensors Actuators B 218:303–309
44. Adam T, Hashim U (2015) Highly sensitive silicon nanowire biosensor with novel liquid gate control for detection of specific single-stranded DNA molecules. Biosens Bioelectron 67:656–661
45. Lee J, Jang J, Choi B, Yoon J, Kim J-Y, Choi Y-K, Kim DM, Kim DH, Choi S-J (2015) A highly responsive silicon nanowire/amplifier MOSFET hybrid biosensor. Sci Rep 5:12286
46. Yen L-C, Pan T-M, Lee C-H, Chao T-S (2016) Label-free and real-time detection of ferritin using a horn-like polycrystalline-silicon nanowire field-effect transistor biosensor. Sensors Actuators B 230:398–404
47. Rahman SFA, Yusof NA, Hashim U, Hushiarian R, Nuzaihan MNM, Hamidon MN, Zawawi RM, Fathil MFM (2016) Enhanced sensing of dengue virus DNA detection using O_2 plasma treated-silicon nanowire based electrical biosensor. Anal Chim Acta 942:74–85
48. Kim K, Park C, Kwon D, Kim D, Meyyappan M, Jeon S (2016) Jeong-Soo Lee, silicon nanowire biosensors for detection of cardiac troponin I (cTnI) with high sensitivity. Biosens Bioelectron 77:695–701
49. Nuzaihan M, Hashim U, Arshad MKM, Kasjoo SR, Rahman SFA, Ruslinda AR, Fathil MFM, Adzhri R, Shahimin MM (2016) Electrical detection of dengue virus (DENV) DNA oligomer using silicon nanowire biosensor with novel molecular gate control. Biosens Bioelectron 83:106–114
50. Presnova G, Presnov D, Krupenin V, Grigorenko V, Trifonov A, Andreeva I, Ignatenko O, Egorov A, Rubtsova M (2017) Biosensor based on a silicon nanowire field-effect transistor functionalized by gold nanoparticles for the highly sensitive determination of prostate specific antigen. Biosens Bioelectron 88:283–289
51. Borgne BL, Pichon L, Salaun AC, Bihan BL, Anne Jolivet-Gougeon S, Martin RR, de Sagazan O (2018) Bacteria electrical detection using 3D silicon nanowires based resistor, Sensors & Actuators:B. Chemical 273:1794–1799
52. Zhou K, Zhao Z, Pan L, Wang Z (2019) Silicon nanowire pH sensors fabricated with CMOS compatible sidewall mask technology. Sensors Actuators: B Chem 279:111–121
53. Zhang H, Kikuchi N, Ohshima N, Kajisa T, Sakata T, Izumi T, Sone H (2020) Design and fabrication of silicon nanowire-based biosensors with integration of critical factors: toward ultrasensitive specific detection of biomolecules. ACS Appl Mater Interfaces 12:51808–51819
54. Gao A, Wang Y, Zhang D, He Y, Zhang L, Liu Y, Wang Y, Song H, Li T (2020) Highly sensitive and selective detection of human-derived volatile organic compounds based on odorant binding proteins functionalized silicon nanowire array. Sensors Actuators: B Chem 309:127762
55. Li D, Chen H, Fan K, Labunov V, Lazarouk S, Yue X, Liu C, Yang X, Dong L, Wang G (2021) A supersensitive silicon nanowire array biosensor for quantitating tumor marker ctDNA. Biosens Bioelectron 181:113147
56. Gautam V, Kumar A, Kumar R, Jain VK, Nagpal S (2021) Silicon nanowires/reduced graphene oxide nanocomposite based novel sensor platform for detection of cyclohexane and formaldehyde. Mater Sci Semicond Process 123:105571
57. Benserhir Y, Anne-Claire Salaün F, Geneste N, Oliviero L, Pichon AJ-G (2022) Silicon nanowires-based biosensors for the electrical detection of Escherichia coli. Biosens Bioelectron 216:114625
58. Zhao W, Hu J, Liu J, Li X, Sun S, Luan X, Zhao Y, Wei S, Li M, Zhang Q, Huang C (2022) Si nanowire bio-FET for electrical and label-free detection of cancer cell-derived exosomes. Microsystems Nanoengineer 8:57
59. Santana JE, Sosa AN, Santiago FD, Miranda A, Perez LA, Trejo A, Salazar F, Cruz-Irisson M (2023) Highly sensitive amphetamine drug detection based on silicon nanowires: theoretical investigation. Surfaces Interfaces 36:102584
60. Santana JE, García KJ, Santiago FD, Miranda A, Perez-Figueroa SE, Gonzalez JE, Perez LA, Cruz-Irisson M (2023) Selective sensing of DNA/RNA nucleobases by metal-functionalized silicon nanowires: a DFT approach. Surfaces Interfaces 36:102529
61. Zheng G, Patolsky F, Cui Y, Wang WU, Lieber CM (2005) Multiplexed electrical detection of cancer markers with nanowire sensor arrays. Nat Biotechnol 23:1294–1301
62. Abiri H, Abdolahad M, Gharooni M, Hosseini SA, Janmaleki M, Azimi S, Hosseini M, Mohajerzadeh S (2015) Monitoring the spreading stage of lung cells by silicon nanowire electrical cell impedance sensor for cancer detection purposes. Biosens Bioelectron 68:577–585
63. Chen Y, Guo J, Muhammad H, Kang Y, Ary SK (2016) CMOS-compatible silicon-nanowire-based coulter counter for cell enumeration. IEEE Trans Biomed Eng 63:311–315
64. Ouhibi A, Raouafi A, Lorrain N, Guendouz M, Raouafi N, Moadhen A (2021) Functionalized SERS substrate based on silicon nanowires for rapid detection of prostate specific antigen, Sensors & Actuators:B. Chemical 330:129352
65. Lu Z, Liu T, Zhou X, Yang Y, Liu Y, Zhou H, Wei S, Zhai Z, Wu Y, Sun F, Wang Z, Li T, Hong J (2022) Rapid and quantitative detection of tear MMP-9 for dry eye patients using a novel silicon nanowire-based biosensor. Biosens Bioelectron 214:114498
66. Vu C-A, Lai H-Y, Chang C-Y, Chan W-H, Chen W-Y (2022) Optimizing surface modification of silicon nanowire field-effect transistors by polyethylene glycol for MicroRNA detection. Colloids Surfaces B:Biointerfaces 209:112142

67. Muratore KA, Zhou D, Du JJ, Chlystek JS, Motesadi K, Larsen EK, Molgora BM, Lee TC, Pamarti S, Erramilli S, Mohanty P (2023) Alanine aminotransferase assay biosensor platform using silicon nanowire field effect transistors. Commun Eng 2:8
68. Lehoucq G, Bondavalli P, Xavier S, Legagneux P, Abbyad P, Baroud CN, Pribat D (2012) Highly sensitive pH measurements using a transistor composed of a large array of parallel silicon nanowires. Sensors Actuators B 171–172:127–134
69. Lale A, Grappin A, Lecestre A, Mazenq L, Launay J, Temple-Boyer P (2023) Top-down integration of suspended $N^+/P/N^+$ silicon-nanowire-based ion-sensitive field effect transistors for pH analysis at the submicronic scale. Thin Solid Films 764:139609
70. Li H-H, Yang C-E, Kei C-C, Chung-Yi S, Dai W-S, Tseng J-K, Yang P-Y, Chou J-C, Cheng H-C (2013) Coaxial-structured ZnO/silicon nanowires extended-gate field-effect transistor as pH sensor. Thin Solid Films 529:173–176
71. Cho S-K, Cho W-J (2021) Ultra-high sensitivity pH-sensors using silicon nanowire channel dual-gate field-effect transistors fabricated by electrospun polyvinylpyrrolidone nanofibers pattern template transfer. Sensors Actuators: B. Chem 326:128835
72. Zhou K, Zhao Z, Yu P, Wang Z (2020) Highly sensitive pH sensors based on double-gate silicon nanowire field effect transistors with dual-mode amplification, Sensors & Actuators:B. Chemical 320:128403
73. Oh JY, Jang H-J, Cho W-J, Islam MS (2012) Highly sensitive electrolyte-insulator-semiconductor pH sensors enabled by silicon nanowires with Al_2O_3/SiO_2 sensing membrane. Sensors Actuators B 171–172:238–243
74. Lin J-C, Huang B-R, Yang Y-K (2013) IGZO nanoparticle-modified silicon nanowires as extended-gate field-effect transistor pH sensors. Sensors Actuators B 184:27–32
75. Park I, Li Z, Li X, Pisano AP, Williams RS (2007) Towards the silicon nanowire-based sensor for intracellular biochemical detection. Biosens Bioelectron 22:2065–2070
76. Lu N, Gao A, Dai P, Mao H, Zuo X, Fan C, Wang Y, Li T (2015) Ultrasensitive detection of dual cancer biomarkers with integrated CMOS-compatible nanowire arrays. Anal Chem 87:11203–11208
77. Zhu K, Zhang Y, Li Z, Zhou F, Feng K, Dou H, Wang T (2015) Simultaneous detection of α-fetoprotein and Carcinoembryonic antigen based on Si nanowire field-effect transistors. Sensors 15:19225–19236
78. Yang X, Fan Y, Wu Z, Liu C (2019) A silicon nanowire Array biosensor fabricated by complementary metal oxide semiconductor technique for highly sensitive and selective detection of serum Carcinoembryonic antigen. Micromachines 10:764
79. Gao A, Yang X, Tong J, Zhou L, Wang Y, Zhao J, Mao H, Li T (2017) Multiplexed detection of lung cancer biomarkers in patients serum with CMOS-compatible silicon nanowire arrays. Biosens Bioelectron 91:482–488
80. Chen H-C, Chen Y-T, Tsai R-Y, Chen M-C, Chen S-L, Xiao M-C, Chen C-L, Hua M-Y (2015) A sensitive and selective magnetic graphene composite-modified polycrystalline-silicon nanowire field-effect transistor for bladder cancer diagnosis. Biosens Bioelectron 66:198–207
81. Malsagova KA, Ivanov YD, Pleshakova TO, Kaysheva AL, Shumov ID, Kozlov AF, Archakov AI, Popov VP, Fomin BI, Latyshev AV (2015) A SOI-nanowire biosensor for the multiple detection of D-NFATc1 protein in the serum. Anal Methods 7:8078–8085
82. Pham VB, Le TTT, Phan TNK, Nguyen TT, Dang CM (2018) Application of silicon nanowire for detection and quantitative analysis of alpha-fetoprotein biomarker. Int J Nanotechnol 15:1–3
83. Yang C-Y, Chiang H-C, Kuo C-J, Hsu C-W, Chan S-F, Lin Z-Y, Lin C-H, Chen Y-T (2018) Hepatocellular carcinoma diagnosis by detecting α-Fucosidase with a silicon nanowire field-effect transistor biosensor. ECS J Solid State Sci Technol 7:Q3153–Q3158
84. Zida SI, Chu-Chun Yang YL, Khung Y-DL (2020) Fabrication and characterization of an Aptamer-based N-type silicon nanowire FET biosensor for VEGF detection. J Med Biol Eng 40:601–609
85. Tran DP, Wolfrum B, Stockmann R, Pai J-H, Pourhassan-Moghaddam M, Offenhäusser A, Thierry B (2015) CMOS compatible silicon nanowires on-a-Chip: fabrication and pre-clinical validation for the detection of a cancer prognostic protein marker in serum. Anal Chem 87:1662–1668
86. Puppo F, Doucey M-A, Delaloye J-F, Moh TSY, Pandraud G, Sarro PM, De Micheli G, Carrara S (2016) SiNW-FET in-air biosensors for high sensitive and specific detection in breast tumor extract. IEEE Sensors J 16:3374–3381
87. Lu N, Gao A, Dai P, Li T, Wang Y, Gao X, Song S, Fan C, Wang Y (2013) Ultra-sensitive nucleic acids detection with electrical nanosensors based on CMOS-compatible silicon nanowire field-effect transistors. Methods 63:212–218
88. Gao A, Lu N, Wang Y, Dai P, Li T, Gao X, Wang Y, Fan C (2012) Enhanced sensing of nucleic acids with silicon nanowire field effect transistor biosensors. Nano Lett 12:5262–5268
89. Malsagova KA, Pleshakova TO, Galiullin RA, Kozlov AF, Romanova TS, Shumov ID, Popov VP, Tikhonenko FV, Glukhov AV, Smirnov AY, Gadzhieva OA, Bashiryan BA, Shimansky VN, Archakov AI, Ivanov YD (2020) SOI-nanowire biosensor for the detection of Glioma-associated miRNAs in plasma. Chemosensors 8:95
90. Kruchinina MV, Prudnikova YI, Kurilovich SA, Gromov AA, Kruchinin VN, Atuchin VV, Naumova OV, Spesivtsev EV, Volodin V, Peltek SE, Shuvalov GV, Vladimir G (2017) Ellipsometry, raman spectroscopy and soi-nanowire biosensor in diagnosis of colorectalcancer. Siberian J Oncol 16:32–41
91. Capua L, Sprunger Y, Elettro H, Risch F, Grammoustianou A, Midahuen R, Ernst T, Barraud S, Gill R, Ionescu AM (2022) Label-free C-reactive protein Si nanowire FET sensor arrays with super-Nernstian Back-gate operation. IEEE Trans Electron Devices 69:2159–2165
92. Shen F, Tan M, Wang Z, Yao M, Xu Z, Wu Y, Wang J, Guo X, Zhu T (2011) Integrating silicon nanowire field effect transistor, microfluidics and air sampling techniques for real-time monitoring biological aerosols. Environ Sci Technol 45:7473–7480
93. Shen F, Wang J, Xu Z, Wu Y, Chen Q, Li X, Jie X, Li L, Yao M, Guo X, Zhu T (2012) Rapid flu diagnosis using silicon nanowire sensor. Nano Lett 12:3722–3730
94. Sreejith S, Ajayan J, Reddy NVU, Devasenapati B, Rebelli S (2024) Analysis of Covid-19 CT chest image classification using Dl4jMlp classifier and multilayer perceptron in WEKA environment, current medical. Imaging 20:e170423215872
95. Seo G, Lee G, Kim MJ, Baek S-H, Choi M, Ku KB, Lee C-S, Jun S, Park D, Kim HG, Kim S-J, Lee J-O, Kim BT, Park EC, Kim SI (2020) Rapid detection of COVID-19 causative virus (SARSCoV-2) in human nasopharyngeal swab specimens using field-effect transistor-based, vol 14, Biosensor, ACS Nano, pp 5135–5142
96. Wasfi A, Awwad F, Qamhieh N, Murshidi BA, Palakkott AR, Gelovani JG (2022) Real-time COVID-19 detection via graphite oxide-based field-effect transistor biosensors decorated with Pt/Pd nanoparticles. Sci Rep 12:18155
97. Poghossian A, Jablonski M, Molinnus D, Wege C, Schöning MJ (2020) Field-effect sensors for virus detection: from Ebola to SARS-CoV-2 and plant viral enhancers. Front Plant Sci 11:598103

98. Samson R, Navale GR, Dharne MS (2020) Biosensors:frontiers in rapid detection of COVID-19, 3. Biotech 10:385
99. Wasfi A, Awwad F, Gelovani JG, Qamhieh N, Ayesh AI (2022) COVID-19 detection via silicon nanowire field-effect transistor: setup and Modeling of its function. Nanomaterials 12:2638
100. Gao B, Chavez RAR, Malkawi WI, Keefe DW, Smith R, Haim H, Salem AK, Toor F (2022) Sensitive detection of SARS-CoV-2 spike protein using vertically-oriented silicon nanowire array-based biosensor. Sensing Bio-Sensing Res 36:100487
101. Chi-Chang W (2022) Polycrystalline silicon nanowire field effect transistor biosensors for SARS-CoV-2 detection. J Electrochem Soc 169:077514
102. Miranda A, de Santiago F, Pérez LA, Cruz-Irisson M (2017) Silicon nanowires as potential gas sensors: a density functional study. Sensors Actuators B 242:1246–1250
103. Akbari-Saatlu M, Procek M, Mattsson C, Thungström G, Nilsson H-E, Xiong W, Xu B, Li Y, Radamson HH (2020) Silicon nanowires for gas sensing. A Review, Nanomaterials 10:2215
104. Paska Y, Haick H (2012) Interactive effect of hysteresis and surface chemistry on gated silicon nanowire gas sensors. ACS Applied Materials Interfaces 4:2604–2617
105. Hsu H-F, Chen C-A, Liu S-W, Tang C-K (2017) Fabrication and gas-sensing properties of Ni-silicide/Si nanowires. Nanoscale Res Lett 12:182
106. Raman S, Ravi Sankar A, Sindhuja M (2023) Advances in silicon nanowire applications in energy generation, storage, sensing, and electronics: a review. Nanotechnology 34:182001
107. Wan J, Deng S-R, Yang R, Shu Z, Lu B-R, Xie S-Q, Chen Y, Huq E, Liu R, Qu X-P (2009) Silicon nanowire sensor for gas detection fabricated by nanoimprint on SU8/SiO_2/PMMA trilayer. Microelectron Eng 86:1238–1242
108. Gao C, Deng S-R, Wan J, Lu B-R, Liu R, Huq E, Qu X-P, Chen Y (2010) 22 nm silicon nanowire gas sensor fabricated by trilayer nanoimprint and wet etching. Microelectron Eng 87:927–930
109. Skucha K, Fan Z, Jeon K, Javey A, Boser B (2010) Palladium/silicon nanowire Schottky barrier-based hydrogen sensors. Sensors Actuators B 145:232–238
110. Gao C, Xu Z-C, Deng S-R, Wan J, Chen Y, Liu R, Huq E (2011) Xin-Ping Qu, silicon nanowires by combined nanoimprint and angle deposition for gas sensing applications. Microelectron Eng 88:2100–2104
111. Yang L, Lin H, Zhang Z, Cheng L, Ye S, Shao M (2013) Gas sensing of tellurium-modified silicon nanowires to ammonia and propylamine. Sensors Actuators B 177:260–264
112. Wu Y, Hu M, Qin Y, Wei X, Ma S, Yan D (2014) Enhanced response characteristics of p-porous silicon (substrate)/p-TeO_2(nanowires) sensor for NO_2detection. Sensors Actuators B 195:181–188
113. Naama S, Hadjersi T, Keffous A, Nezzal G (2015) CO_2 gas sensor based on silicon nanowires modified with metal nanoparticles. Mater Sci Semicond Process 38:367–372
114. Qin Y, Liu D, Zhang T, Cui Z (2017) Ultrasensitive silicon nanowire sensor developed by a special Ag modification process for rapid NH_3 detection. ACS Appl Mater Interfaces 9:28766–28773
115. Qin Y, Wang Z, Liu D, Wang K (2017) Dendritic composite array of silicon nanowires/WO_3 nanowires for sensitive detection of NO_2 at room temperature. Mater Lett 207:29–32
116. Qiang X, Hu M, Zhao B, Qin Y, Zhang T, Zhou L, Liang J (2018) Preparation of porous silicon/Pd-loaded WO_3 nanowires for enhancement of ammonia sensing properties at room temperature. Mater Sci Semicond Process 79:113–118
117. Yun J, Ahn J-H, Moon D-I, Choi Y-K, Park I (2019) Joule heated and suspended silicon nanowire based sensor for low-power and stable hydrogen detection. ACS Appl Mat Interfaces 11:42349–42357
118. Qin Y, Zang J (2021) Stable clusters array of silicon nanowires developed by top-plating technique as a high-performance gas sensor. Physica E:Low-dimensional Syst Nanostruc 127:114508
119. Mukherjee A, Gnaim M, Tov IS, Hargreaves L, Hayon J, Shluger A, Rosenwaks Y (2021) Ultrasensitive hydrogen detection by electrostatically formed silicon nanowire decorated by palladium nanoparticles. Sensors Actuators:B Chem 346:130509
120. Qin Y, Wang X, Zang J (2021) Room-temperature ethanol sensor based on ZIF-67 modified silicon nanowires with expanded detection range and enhanced moisture resistance. Chem Phys Lett 765:138302
121. Dwivedi P, Dhanekar S, Das S (2021) Near room temperature sensing by In_2O_3 decorated silicon nanowires for sensitive detection of ethanol. IEEE Sensors J 21:7275–7282
122. Song X, Hu R, Xu S, Liu Z, Wang J, Shi Y, Xu J, Chen K, Yu L (2021) Highly sensitive ammonia gas detection at room temperature by Integratable silicon nanowire field-effect sensors. ACS Appl Mater Interfaces 13:14377–14384
123. Kashyap V, Pawar H, Kumar C, Chaudhary N, Saxena K (2022) Analysis of synthesized doped vertical silicon nanowire arrays for effective sensing of nitrogen dioxide: as gas sensors. Front Mat 9:1022317
124. Nath P, Sarkar D (2022) Ammonia sensing by silicon nanowires (SINWs) obtained through metal assisted electrochemical etching. Mat Today: Proceed 57:224–227
125. Chaujar R, Yirak MG (2023) Sensitivity investigation of Junctionless gate-all-around silicon nanowire field-effect transistor-based hydrogen gas sensor. Silicon 15:609–621
126. Demami F, Ni L, Rogel R, Salaun AC, Pichon L (2012) Silicon nanowires based resistors as gas sensors. Sensors Actuators B 170:158–162
127. Huang J, Zhu Y, Zhong H, Yang X, Li C (2014) Dispersed CuO nanoparticles on a silicon nanowire for improved performance of nonenzymatic H_2O_2 detection. ACS Appl Mater Interfaces 6:7055–7062
128. Pichon L, Salaün AC, Wenga G, Rogel R, Jacques E (2014) Ammonia sensors based on suspended silicon nanowires. Procedia Eng 87:1003–1006
129. Choi B, Jae-Hyuk Ahn J, Lee J, Yoon J, Lee M, Jeon DM, Kim DH, Kim IP, Choi S-J (2015) A bottom-gate silicon nanowire field-effect transistor with functionalized palladium nanoparticles for hydrogen gas sensors. Solid State Electron 114:76–79
130. Zhang W, Hu M, Liu X, Wei Y, Li N, Qin Y (2016) Synthesis of the cactus-like silicon nanowires/tungsten oxide nanowires composite for room-temperature NO_2 gas sensor. J Alloys Compd 679:391–399
131. Lee K, Dae-Hyun Baek H, Na J, Choi JK (2018) Simple fabrication method of silicon/tungsten oxide nanowires heterojunction for NO_2 gas sensors. Sensors Actuators B 265:522–528
132. Ocak YS, Zeggar ML, Genisel MF, Uzun NU, Aida MS (2021) CO_2 sensing behavior of vertically aligned Si nanowire/ZnO structures. Mater Sci Semicond Process 134:106028
133. Jeribi M, Nafie N, Boujmil MF, Bouaicha M (2021) Response modulation of silicon nanowires-based sensor to carbon number in petroleum vapor detection. Fuel 304:121260
134. Zhao S, Li Z, Wang G, Liao J, Lv S, Zhu Z (2018) Highly enhanced response of MoS_2/porous silicon nanowire heterojunctions to NO_2 at room temperature. RSC Adv 8:11070–11077
135. Kim J, Oh SD, Kim JH, Shin DH, Kim S, Choi SH (2014) Graphene/Si-nanowire heterostructure molecular sensors. Sci Rep 4:5384
136. Demami F, Ni L, Rogel R, Salaun AC, Pichon L (2010) Silicon nanowires synthesis for chemical sensor applications. Procedia Eng 5:351–354
137. Zhou XT, Hu JQ, Li CP, Ma DDD, Lee CS, Lee ST (2003) Silicon nanowires as chemical sensors. Chem Phys Lett 369:220–224

138. Lee J, Choi B, Hwang S, Lee JH, Park B-G, Park TJ, Kim DM, Kim DH, Choi S-J (2014) Investigation of sensor performance in accumulation- and inversion-mode silicon nanowire pH sensors. IEEE Trans Electron Devices 61:1607-1610
139. Abbas N, Kim J, Yeom J, Lee S, Lu X (2021) Seok-min Kim, monolithic fabrication of vertical silicon nanowire gas sensor with a top porous copper electrode using glancing angle deposition. J Mater Sci Mater Electron 32:5233–5242
140. Cui Y, Wei Q, Park H, Lieber CM (2001) Nanowire nanosensors for highly sensitive and selective detection of biological and chemical species. Science 293:1289–1292
141. Bi X, Wong WL, Ji W, Agarwal A, Balasubramanian N (2008) Kun-Lin Yang, development of electrochemical calcium sensors by using silicon nanowires modified with phosphotyrosine. Biosens Bioelectron 23:1442–1448
142. Bi X, Agarwal A, Balasubramanian N (2008) Kun-Lin Yang, Tripeptide-modified silicon nanowire based field-effect transistors as real-time copper ion sensors. Electrochem Commun 10:1868–1871
143. Bi X, Agarwal A (2009) Kun-Lin Yang, Oligopeptide-modified silicon nanowire arrays as multichannel metal ion sensors. Biosens Bioelectron 24:3248–3251
144. Yin J, Qi X, Yang L, Hao G, Li J, Zhong J (2011) A hydrogen peroxide electrochemical sensor based on silver nanoparticles decorated silicon nanowire arrays. Electrochim Acta 56:3884–3889
145. Yan Q, Wang Z, Zhang J, Peng H, Chen X, Hou H, Liu C (2012) Nickel hydroxide modified silicon nanowires electrode for hydrogen peroxide sensor applications. Electrochim Acta 61:148–153
146. Georgiev YM, Petkov N, McCarthy B, Yu R, Djara V, O'Connell D, Lotty O, Nightingale AM, Thamsumet N, deMello JC, Blake A, Das S, Holmes JD (2014) Fully CMOS-compatible top-down fabrication of sub-50 nm silicon nanowire sensing devices. Microelectron Eng 118:47–53
147. Livi P, Shadmani A, Wipf M, Stoop RL, Rothe J, Chen Y, Calame M, Schönenberger C, Hierlemann A (2014) Sensor system including silicon nanowire ion sensitive FET arrays and CMOS readout. Sensors Actuators B 204:568–577
148. Cao X, Mu L, Chen M, She G (2018) A facile fluorescent sensor based on silicon nanowires for dithionite. Appl Surf Sci 441:388–393
149. Cho S-K, Cho W-J (2021) Highly sensitive and selective sodium ion sensor based on silicon nanowire dual gate field-effect transistor. Sensors 21:4213
150. Daoudi K, Gaidi M, Columbus S, Shameer M, Alawadhi H (2022) Hierarchically assembled silver nanoprism-graphene oxide-silicon nanowire arrays for ultrasensitive surface enhanced Raman spectroscopy sensing of atrazine. Mater Sci Semicond Process 138:106288
151. Luo L, Jie J, Zhang W, He Z, Wang J, Yuan G, Zhang W, Wu LCM (2009) Shuit-Tong Lee, silicon nanowire sensors for Hg^{2+} and Cd^{2+} ions. Appl Phyisics Lett 94:193101
152. Xu W, Mu L, Miao R, Zhang T, Shi W (2011) Fluorescence sensor for Cu(II) based on R6G derivatives modified silicon nanowires. J Lumin 131:2616–2620
153. Clavaguera S, Raoul N, Carella A, Delalande M, Celle C (2011) Jean-Pierre Simonato, development of an autonomous detector for sensing of nerve agents based on functionalized silicon nanowire field-effect transistors. Talanta 85:2542–2545
154. Chen X, Zhang J, Wang Z, Yan Q, Hui S (2011) Humidity sensing behavior of silicon nanowires with hexamethyldisilazane modification. Sensors Actuators B 156:631–636
155. Wang HY, Wang YQ, Hu QF, Li XJ (2012) Capacitive humidity sensing properties of SiC nanowires grown on silicon nanoporous pillar array. Sensors Actuators B 166-167:451-456
156. Taghinejad H, Taghinejad M, Abdolahad M, Saeidi A, Mohajerzadeh S (2013) Fabrication and modeling of high sensitivity humidity sensors based on doped silicon nanowires. Sensors Actuators B 176:413–419
157. Zhang S, Wang T, Lou L, Tsang WM, Sawada R, Kwong D-L, Lee C (2014) Annularly grooved diaphragm pressure sensor with embedded silicon nanowires for low pressure application. J Microelectromechanical Syst 23:1396–1407
158. Wang Z, Song C, Yin H, Zhang J (2015) Capacitive humidity sensors based on zinc oxide nanorods grown on silicon nanowires arrays at room temperature. Sensors Actuators A 235:234–239
159. Chen G, Yu B, Li X, Xu X, Li Z, Huang R, Li M (2019) Selective-assembling hybrid Porphyrin-silicon nanowire field-effect transistor (PSNFET) for photonic sensor. IEEE Electron Device Lett 40:812–814
160. Kim C, Ahn H, Ji T (2020) Flexible pressure sensors based on silicon nanowire array built by metal-assisted chemical etching. IEEE Electron Device Lett 41:1233–1236
161. Rhee J, Kim H, Yang H, Kim S, Lee H (2021) Under-display optical proximity sensor with silicon nanowires. IEEE Sensors J 21:20239–20247
162. Yang Y, Duan S, Xiao W, Zhao H (2022) Silver nanowire-based stretchable strain sensors with hierarchical wrinkled structures. Sensors Actuators: A Physical 343:113653
163. Lou L, Zhang S, Lim L, Woo-Tae Park H, Feng D-LK, Lee C (2011) Characteristics of NEMS Piezoresistive silicon nanowires pressure sensors with various diaphragm layers. Procedia Eng 25:1433–1436
164. Li H, Zhang J, Tao B, Wan L, Gong W (2009) Investigation of capacitive humidity sensing behavior of silicon nanowires. Phys E 41:600–604
165. Lee J, Jin-Moo Lee JH, Lee WH, Lee MU, Byung-Gook Park DM, Kim Y-JJ, Kim DH (2012) Complementary silicon nanowire hydrogen ion sensor with high sensitivity and voltage output. IEEE Electron Device Lett 33:1768–1770
166. Zhang S, Lou L, Gu Y (2017) Development of Silicon Nanowire–Based NEMS Absolute Pressure Sensor through Surface Micromachining. IEEE Electron Device Lett 38:653-656
167. Singh RR, Malviya N, Priye V (2016) Parametric analysis of silicon nanowire optical rectangular waveguide sensor. IEEE Photon Technol Lett 28:2889–2892
168. Nair RS, Perret E, Tedjini S, Baron T (2013) A group-delay-based Chipless RFID humidity tag sensor using silicon nanowires. IEEE Antennas Wireless Propag Lett 12:729–732
169. Mohamedyaseen A, Kumar PS (2022) The fabrication of high-anisotropy silicon nanowires based on MACE method for photonic sensor. Silicon 14:11417–11427
170. Morganti D, Faro MJL, Leonardi AA, Fazio B, Conoci S, Irrera A (2022) Luminescent silicon nanowires as novel sensor for environmental air quality control. Sensors 22:8755
171. Cheng W, Yu L, Kong D, Yu Z, Wang H, Ma Z, Wang Y, Wang J, Pan L, Shi Y (2018) Fast response and low hysterisis fexible pressure sensor base on silicon nanowires. IEEE Electron Device Lett 39:1069–1072

Publisher's Note Springer Nature remains neutral with regard to jurisdictional claims in published maps and institutional affiliations.

Springer Nature or its licensor (e.g. a society or other partner) holds exclusive rights to this article under a publishing agreement with the author(s) or other rightsholder(s); author self-archiving of the accepted manuscript version of this article is solely governed by the terms of such publishing agreement and applicable law.